Graduate School ETD Form 9
(Revised 12/07)

PURDUE UNIVERSITY
GRADUATE SCHOOL
Thesis/Dissertation Acceptance

This is to certify that the thesis/dissertation prepared

By Spandana Gannavaram

Entitled
Modeling and Design Optimization of a Microfluidic Chip for Isolation of Rare Cells

For the degree of Master of Science in Mechanical Engineering

Is approved by the final examining committee:

LIKUN ZHU
Chair

WHITNEY YU

JIAN XIE

To the best of my knowledge and as understood by the student in the *Research Integrity and Copyright Disclaimer (Graduate School Form 20)*, this thesis/dissertation adheres to the provisions of Purdue University's "Policy on Integrity in Research" and the use of copyrighted material.

Approved by Major Professor(s): LIKUN ZHU

Approved by: SOHEL ANWAR 10/04/2013
Head of the Graduate Program Date

MODELING AND DESIGN OPTIMIZATION OF A MICROFLUIDIC CHIP FOR ISOLATION OF RARE CELLS

A Thesis

Submitted to the Faculty

of

Purdue University

by

Spandana Gannavaram

In Partial Fulfillment of the

Requirements for the Degree

of

Master of Science in Mechanical Engineering

December 2013

Purdue University

Indianapolis, Indiana

To my family and friends, for your endless support.

ACKNOWLEDGMENTS

I would like to express my deep gratitude to my advisor, Dr. Likun Zhu for his invaluable time, guidance, motivation to better my work and constant supervision for the entire course of the research work. Most of all, I would like to thank him for having given me the opportunity to work under him.

I would like to acknowledge my advisory committee members Dr. Whitney Yu and Dr. Jian Xie, for their helpful suggestions and recommendations on the thesis work. Dr. Whitney Yu made me aware of important details which I would have otherwise missed and for this I am very thankful to her.

I would like to extend my thanks to the faculty, staff and students of the Department of Mechanical Engineering for assisting in the completion of this thesis work.

Finally, a simple thank you would not suffice for the support and motivation given by my parents and family, because of whom I am here today. A heartfelt thanks to my dear friends, who have always been there for me.

TABLE OF CONTENTS

LIST OF TABLES

LIST OF FIGURES

Figure Page

Figure Page

LIST OF SYMBOLS

m	Mass
Re	Reynolds number
Pe	Peclet number
a	Radius of solid core
b	Radius of micropost
$\vec{V}$	velocity vector
u	Velocity component in x-direction
v	Velocity component in y-direction
w	Velocity component in z-direction
μ	Dynamic viscosity
ν	Kinematic viscosity
ρ	Density
K	Permeability
P	Pressure
τ	Shear stress
ψ	Stream function
u_m	Mean velocity
Da	Darcy number
α	Volume fraction of cylinders

LIST OF ABBREVIATIONS

1D	One-dimensional
2D	Two-dimensional
CTC	Circulating Tumor Cells
PSMA	Prostate-Specific Membrane Antigen
GEDI	Geometrically Enhanced Differential Immunocapture
VACNT	Vertically Aligned Carbon Nanotubes
SiNP	Silicon Nanopillars
DRIE	Deep Reactive-Ion Etching
PCTC	Prostate Circulating Tumor Cells
DEP	Dielectrophoresis
DACS	DEP-Activated Cell Sorter

ABSTRACT

Gannavaram, Spandana. M.S.M.E, Purdue University, December 2013. Modeling and Design Optimization of a Microfluidic Chip for Isolation of Rare Cells. Major Professor: Likun Zhu.

Cancer is still among those diseases that prominently contribute to the numerous deaths that are caused each year. But as technology and research is reaching new zeniths in the present times, cure or early detection of cancer is possible. The detection of rare cells can help understand the origin of many diseases. The current study deals with one such technology that is used for the capture or effective separation of these rare cells called Lab-on-a-chip microchip technology. The isolation and capture of rare cells is a problem uniquely suited to microfluidic devices, in which geometries on the cellular length scale can be engineered and a wide range of chemical functionalizations can be implemented. The performance of such devices is primarily affected by the chemical interaction between the cell and the capture surface and the mechanics of cell-surface collision and adhesion. This study focuses on the fundamental adhesion and transport mechanisms in rare cell-capture microdevices, and explores modern device design strategies in a transport context. The biorheology and engineering parameters of cell adhesion are defined; chip geometries are reviewed. Transport at the microscale, cell-wall interactions that result in cell motion across streamlines, is discussed.

We have concentrated majorly on the fluid dynamics design of the chip. A simplified description of the device would be to say that the chip is at micro scale. There are posts arranged on the chip such that the arrangement will lead to a higher capture of rare cells. Blood consisting of rare cells will be passed through the chip and the posts will pose as an obstruction so that the interception and capture efficiency of the rare cells increases. The captured cells can be observed by fluorescence microscopy.

As compared to previous studies of using solid microposts, we will be incorporating a new concept of cylindrical shell micropost. This type of micropost consists of a solid inner core and the annulus area is covered with a forest of silicon nanopillars. Utilization of such a design helps in increasing the interception and capture efficiency and reducing the hydrodynamic resistance between the cells and the posts.

Computational analysis is done for different designs of the posts. Drag on the microposts due to fluid flow has a great significance on the capture efficiency of the chip. Also, the arrangement of the posts is important to contributing to the increase in the interception efficiency. The effects of these parameters on the efficiency in junction with other factors have been studied and quantified. The study is concluded by discussing design strategies with a focus on leveraging the underlying transport phenomena to maximize device performance.

1. INTRODUCTION

1.1 Rare Cells: Circulating Tumor Cells

Cancer is a leading cause of death worldwide and accounts for millions of deaths every year. For many years now the origin of cancer has been a question that is yet to be completely answered and ways to treat this disease have produced few good solutions. A hundred years ago, with the discovery of radioactivity, people saw an association between cancer and exposure to X-rays or radioactive elements. More recently, some scientists proposed that cancer was caused by viruses. Others said that cancer arose from inborn genetic flaws. Until recently, there was no unifying theory to tie together these observations. And no matter what the cause, for most of history there was very little that doctors could do to treat cancer effectively. In the last century there have been moderate improvements in treating cancer, and in the last decade or two researchers have come to a unifying overview of how cancers arise. This unified view assumes that the growth of tissues and the reproduction of cells in our bodies are carefully regulated through the action of key sets of DNA instructions. When those DNA sequences are disrupted–whether through viruses, environmental causes like radiation or toxins, mutations transcription errors or inborn genetic flaws, cell reproduction becomes less well regulated. Eventually, those changes can produce the rapidly reproducing, self-protective and opportunistic cells that typify cancer [1, 2, 5, 6].

Metastasis is a complex process that involves the spread of a tumor or cancer to distant parts of the body from its original site. However, this is a difficult process. To successfully colonize a distant area in the body a cancer cell must complete a series of steps before it becomes a clinically detectable lesion. Metastasis is one of three hallmarks of malignancy or cancer as opposed to a benign tumor. Most tumors

and other neoplasms can metastasize. The degree of ability to spread, however, varies between different types of tumors. Some organs are more prone than others to metastasis of primary tumors. The theory for metastasis states that cancer cells find survival outside their primary suites difficult. To spread they need to find a location with similar characteristics [5].

Rare cells in cancer research can comprise of stem cells and circulating tumor cells (CTCs). Stem cells are cells that reproduce themselves and give rise to other kinds of cells. Most cells in our bodies are not stem cells. Some, like blood precursor cells, can give rise to various kinds of blood cells, but cannot reproduce themselves. Research has shown that cancer cells are not all the same. Within a malignant tumor or among the circulating cancerous cells of leukemia, there can be a variety of types of cells. The stem cell theory of cancer proposes that among all cancerous cells, a few acts as stem cells that reproduce themselves and sustain the cancer, much like normal stem cells normally renew and sustain our organs and tissues. In this view, cancer cells that are not stem cells can cause problems, but they cannot sustain an attack on our bodies over the long term. The idea that cancer is primarily driven by a smaller population of stem cells has important implications [8,9]. For instance, many new anti-cancer therapies are evaluated based on their ability to shrink tumors, but if the therapies are not killing the cancer stem cells, the tumor will soon grow back (often with a vexing resistance to the previously used therapy). An analogy would be a weeding technique that is evaluated based on how low it can chop the weed stalks; but no matter how low the weeks are cut, if the roots arent taken out, the weeds will just grow back. Another important implication is that it is the cancer stem cells that give rise to metastases i.e. when cancer travels from one part of the body to another and can also act as a reservoir of cancer cells that may cause a relapse after surgery, radiation or chemotherapy has eliminated all observable signs of a cancer [7].

For a promising treatment of cancer, early diagnosis is important. This is done so by detecting the rare cells such as circulating tumor cells (CTCs) in patient blood. CTCs are cells detached from a primary tumor and circulated in the bloodstream

that can serve as important cancer biomarkers. However, they are rare, comprising only 1 out of 109 haematologic cells in 1 mL blood sample. Methods that can sensitively and accurately detect CTCs are, therefore, in great demand. Among all the tools developed till now, microfluidic chips with high-affinity ligands have provided an easy and inexpensive way to capture and detect CTCs. Circulating tumor cells have been identified in peripheral blood from cancer patients and are probably the origin of inflexible metastatic disease. Although extremely rare, CTCs represent a potential alternative to invasive surgeries as a source of tumor tissue for the detection, characterization and monitoring of non-haematologic cancers. The ability to identify, isolate, propagate and molecularly characterize CTC subpopulations could further the discovery of cancer stem cell biomarkers and expand the understanding of the biology of metastasis. Current strategies for isolating CTCs are limited to complex analytic approaches that generate very low yield and purity [4].

Recent lab-on-a-chip technologies include the development of a silicon microchip for capturing CTCs using antibodies as capturing ligands. Various research groups have employed microfluidic device with different structures to increase the capture efficiency of CTCs. This work aims to design, fabricate, and characterize a micro scale design that will be integrated into microfluidic devices to enhance particle and rare cell capture efficiency. Despite the significant progress achieved in development of cell capture techniques, the enhancement in capture efficiency is still limited and often accompanied with drawbacks such as low throughput, low selectivity, pre-diluting requirement, and cell viability issues [10].

We have studied effects of fluid flow and its influence on the capture efficiency for two different configurations of microposts. They are a) solid micropost and b) solid core with permeable shell micropost. The novelty of this particular field of cancer research is the incorporation of the solid core with permeable shell micropost design. With the support of computational analysis and simulations, the efficiency of this design will be quantified and the study will be directed towards reducing the problems of low throughput, selectivity and increasing binding and capture efficiency.

This work will include the various fabrication processes of the devices and then each of the designs will then be compared for the respective efficiencies of the capture of rare cells [21].

1.2 Literature Review

1.2.1 Microfluidics and Lab-on-a-chip Technology for Cell Separation

Diminishment of macroscale laboratory operations can expand the scope and functionalization of existing bioassays, separation technologies and chemical synthesis techniques. Although a reduction in size to the micrometer scale will usually not change the nature of molecular reactions, laws of scale for surface per volume, molecular diffusion and heat transport enable dramatic increases in throughput. Microfluidic chips have been widely used to provide small volumes and fluid connections and could eventually outperform conventionally used robotic fluid handling. Moreover, completely novel applications without a macroscopic equivalent have recently been developed [19, 21, 23].

Microfluidic chips deals with the behavior, precise control and manipulation of fluids that are geometrically constrained to a small, typically sub-millimeter scale. The volume of fluid that can be handled by these chips can be as small as Pico liters. The size of the channels is in the range of a few micrometers and therefore facilitates the handling of such low volumes of fluid. Microfluidic devices require only a small amount of sample and reagents for processing and possesses large surface to volume ratios. In addition, fast reaction times and ease of automation make microfluidic devices ideal for application in biomedical engineering scenarios [12].

The Reynolds number, Re, for most microfluidic applications is less than 1 and simplified forms of the Navier-Stokes equation are substantiated; Stokes flow conditions are often satisfied. The characteristics of the strictly laminar flow regime alter the design process for microfluidic components, in particular micro-reactors and micro-mixers. Scaling down the size creates a surface force dominating environment.

Surface forces, such as capillary and electrostatic forces, scale to the first or second order of the characteristic length while body forces, gravity and magnetic forces, scale to the third power. According to the same principle, diffusion time and velocity time scale to the second power and first power of the length, respectively. The Peclet number,Pe scales approximately to the first power; however, it isnt uncommon for a wide range of Pe values to be encountered in microfluidics, making generalizations about the relative advection and diffusion properties difficult [8].

Four principal methods are used for generating flow in microfluidic systems: 1. pressure force, 2.electroosmotic force, 3. centrifugal force, and 4. capillary force. Pressure driven flow is very common; the flow characteristics are well reported and predictable in the laminar regime. The fluid pumping is accomplished by external high-precision syringe pumps or by on-chip peristaltic or micro-pneumatic pumping techniques. Centrifugal force is rarely incorporated as the primary microfluidic flow technique due to the requirement for high-speed rotation. The Gyrolab microlaboratory developed by Gyros is an example of a device using this mechanism for the analysis of proteins. Capillary forces become very significant at the microscale and can rapidly propel fluids through networks with appropriate hydrophilic surface conditions. Passive valves have been developed by patterning hydrophobic sections in an otherwise hydrophilic network, but capillary action is difficult to harness for continuous flow operation [24, 25].

Microfluidics has been widely used in the development of lab-on-chip devices, particularly for drug screening in the pharmaceutical industry and in the development of micro-arrays. The technology is rapidly maturing following vigorous research effort over the last 20 years. In the near future, we will see a growing trend towards the production of tailored microfluidic devices which satisfy particular needs, which may be clinical, pharmaceutical, or biotechnological [37–39].

One of the most promising applications of microfluidics in biomedical engineering is in point-of-care diagnosis. In the important sample preparation stage, targeted biological cells need to be separated from other substances in the sample. Conventionally,

cells can be separated in a fluidic suspension, based on size, density, electrical charge, light-scattering properties, and antigenic surface properties. Separating cells according to these metrics can require complex technologies and specialist equipment. Such techniques include centrifuging, fluorescence activated cell sorting, electrophoresis, chromatography, affinity separation and magnetic separation. Microfluidic solutions have been successfully engineered to either integrate into the above techniques, or to function as a standalone device to execute sample preparation tasks [44].

Information about a given cell population can be gained using a variety of cell control, detection, and analysis methods. Furthermore, distinct characteristics of subpopulations can be gathered by analyzing each individual cell from a population, as opposed to averaging the parameters of an entire population. Characterization of the individual cells and intracellular contents is useful for the study of many processes where details of cell behavior and function provide understanding of biological practices and assist in optimization. This function enables far more flexibility in cell diagnostics. For example, the detection and analysis of a particular cell is used in oncology for the diagnosis of chromosomal defects and cancers, such as leukemia, lymphoma, and breast cancer. Pharmacology, drug discovery, and the effects of drugs on bioparticles can be investigated using cellular analysis. Rapid detection of bacteria, such as E. coli, in food or water sources has importance as food transported illnesses and outbreaks are seemingly common. Also, genetics research, environmental monitoring, and immunology, such as the analysis of blood samples and bone marrow samples, benefit from the ability to characterize subpopulations from a larger cellular matrix [13].

In the recent past, this technique of lab-on-a-chip has been extensively applied to the cancer research field. With cancer being one of the most prominent health concerns, the development of new technologies for cancer diagnostics and therapy monitoring is of enormous interest. While traditional therapeutic approaches target primary tumor characteristics, tumor cell dissemination is the most critical aspect in respect of prognosis. To reflect the molecular characteristics of tumor cells, in-

cluding their potential for metastasis development, tumor recurrence, and prognosis, circulating tumor cells (CTCs) in peripheral blood are discussed as relevant markers. CTCs are cells that disseminate from the tumor and may lead to the formation of metastase. Detection of circulating tumor cell analysis in peripheral blood resembles a promising alternative in the progress towards curing cancer [8].

In the literature of the research, many mechanisms have been developed and put into practice for the separation of cells, more specifically CTCs. One such mechanism is the immunomagnetic separation based on capture agent- labeled magnetic beads. An immunomagnetic cell separator, the MagSweeper, gently enriches target cells and eliminates cells that are not bound to magnetic particles. The isolated cells are easily accessible and can be extracted individually based on their physical characteristics to deplete any cells nonspecifically bound to beads. Fundamentally, cell capture occurs when the magnetic force exerted on a labeled cell, F_m, is sufficient to draw the cell to the surface of the magnet. The magnetic force is opposed by a viscous drag force that results from the cells motion relative to that of the surrounding fluid. As the magnet sweeping speed is increased, the region of cell capture around the magnet (i.e., the cross-sectional capture area) will shrink. The details of cell capture in the MagSweeper system are complex, featuring orbital magnet motion, circular fluid flow, nonuniform magnetic field gradients, and variable particle susceptibility.

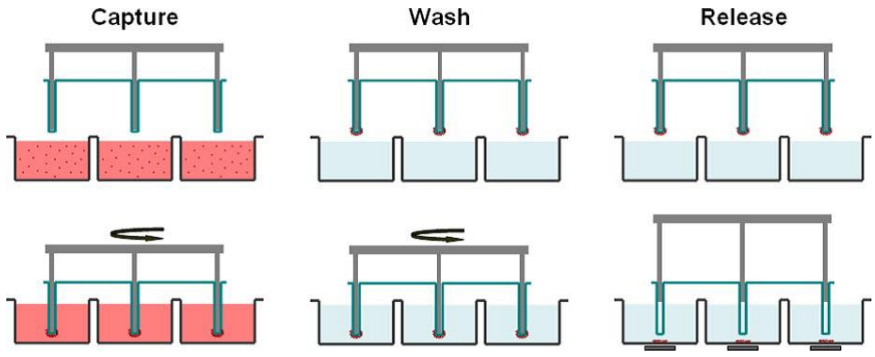

Figure 1.1. The schematic representation of the process of cell capture in the MagSweeper system [12].

The diluted blood samples, which are prelabeled with magnetic particles, are loaded into the capture wells. The magnetic rods covered with plastic sheaths are swept through the well in concentric circular loops at a level 1.5 mm above the bottom of the wells. After sweeping through the whole area of the capture wells, the sheathed magnets are washed in a circular loop to remove loosely bound contaminating cells. The rods are then immersed into a new buffer solution and disengage from the plastic covers. The external magnets located under the wells facilitate release of labeled cells and excess magnetic particles. Another round of capture-wash-release is performed to eliminate the majority of remaining contaminant cells entrapped within excess magnetic particles [9].

A major development in this field was brought about by S. Nagrath and group. They had introduced and developed a circulating tumor cell chip (CTC-chip)which is shown in Fig. 1.2. As stated earlier, microfluidic lab-on-a-chip devices provide unique opportunities for cell sorting and rare-cell detection. They have been successfully used for microfluidic flow cytometry, continuous size-based separation and chromatographic separation. The research group made use of this concept to develop the CTC-chip. In their study, they have discussed the development and application of a microfluidic device that can efficiently and reproducibly isolate CTCs from the blood of patients with common epithelial tumors. The CTC-chip consists of an array of microposts that are made chemically functional with anti-epithelial-cell-adhesion-molecule (EpCAM) antibodies. Anti-EpCAM provides the specificity for CTC capture from unfractionated blood because EpCAM is frequently overexpressed by carcinomas of lung, colorectal, breast, prostate, head and neck, and hepatic origin, and is absent from haematologic cells [8].

3D-nanostructured substrate coated with cancer-cell capture agents (i.e. epithelial cell adhesion molecule antibody, anti-EpCAM) exhibits significantly improved cell-capture efficiency owing to its enhanced local topographic interactions between the silicon nanopillar (SiNP) substrates and nanoscale cellular surface components (e.g., microvilli and filopodia). Such a high-affinity cell assay can be employed to recover

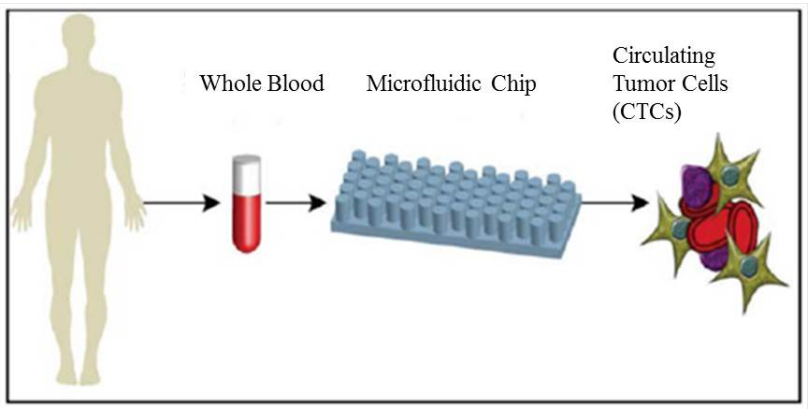

Figure 1.2. One-step process for point-of-care isolation of CTCs from peripheral blood [4].

cancer cells from spiked whole-blood samples, in a stationary device setting, with cell-capture efficiency ranging from 40 to 70%. On the basis of this stationary cell-capture assay, it was anticipated that further improvement of cell-capture performance can be achieved by increasing cellsubstrate contact frequency. By integrating a simple but powerful fluidic handling system, namely a chaotic mixing channel,shown in Fig. 1.3 with a patterned nanostructured substrate, highly efficient CTC capture can be realized by the synergistic effects of enhanced cellsubstrate contact frequency as well as affinity. Although there are several microfluidic platforms capable of achieving improved CTC-capture efficiency, the micropillar based CTC-capture technologies suffer from depth of field issues thus requiring multiple cross-sectional imaging scans to avoid out-of-focus or superimposed images of device immobilized CTCs because of to the vertical depth of the device features [16]. The microfluidic device with an integrated conductivity sensor provides the significant advantage of label-free CTC detection. However, whether the lack of cellular morphology influences pathologic characterization remains to be determined.

The device is composed of two functional components, a patterned silicon nanopillar (SiNP) substrate (1) with anti-EpCAM-coating exhibiting vastly enhanced CTC-

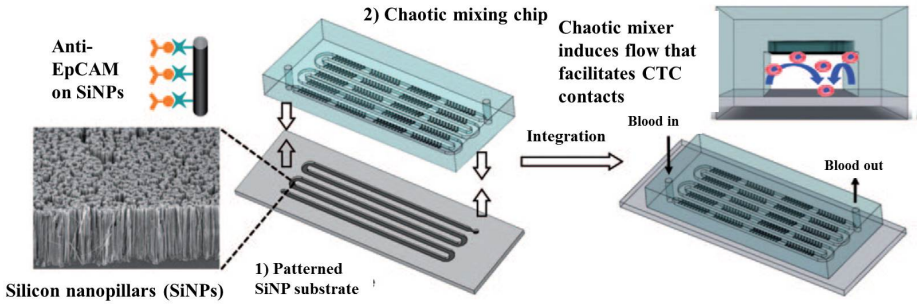

Figure 1.3. (1) Patterned Silicon Nanopillar substrates (2) The chaotic mixing chip that facilitates the cell-post contact [1].

capture affinity, and an overlaid microfluidic chaotic mixing chip (2) capable of promoting cellsubstrate contact frequency.

To efficiently isolate rare cells from complex mixtures, an electrokinetic sorting methodology was developed that exploits dielectrophoresis (DEP) in microfluidic channels. In this approach, the dielectrophoretic amplitude response of rare target cells is modulated by labeling cells with particles that differ in polarization response. Cell mixtures were interrogated in the DEP-activated cell sorter in a continuous-flow manner, wherein the electric fields were engineered to achieve efficient separation between the dielectrophoretically labeled and unlabeled cells. To demonstrate the efficiency of marker-specific cell separation, DEP-activated cell sorting (DACS) was applied for affinity-based enrichment of rare bacteria expressing a specific surface marker from an excess of non-target bacteria that do not express this marker. Rare target cells were enriched by >200-fold in a single round of sorting at a single-channel throughput of 10,000 cells per second. DACS offers the potential for automated, surface marker-specific cell sorting in a disposable format that is capable of simultaneously achieving high throughput, purity, and rare cell recovery [17].

The DACS device was designed and constructed to exploit the differences in dielectrophoretic response between unlabeled and bead-labeled cells. A schematic view of the device design is shown in Fig. 1.4 where the matching electrodes on the top and bottom walls of the microchannel establish an electric field with the highest field

gradient occurring close to the electrodes. The electrodes were fabricated at an angle of 15^0 to the direction of the fluid flow to reduce the nDEP force required for the deflection. As the mixture enters this region, the dielectrophoretically labeled cells are selectively deflected by nDEP. As a result, target cells can be electrokinetically funneled into the collection channel while the unlabeled cells are rejected into the waste channel.

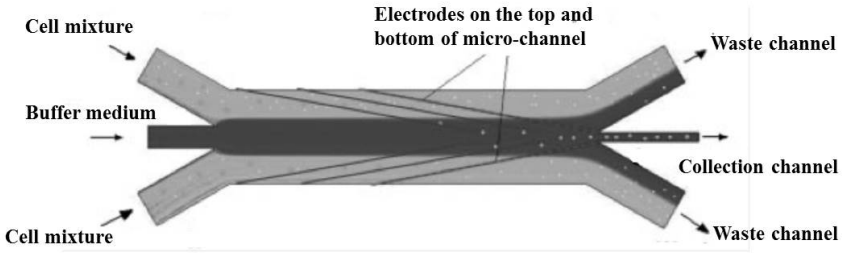

Figure 1.4. The DACS system that is used for specific cell sorting [5].

B.J. Kirby et.al introduced a new technique that demonstrated high-efficiency and high-purity capture of Prostate cancer circulating tumor cells (PCTCs) from peripheral blood samples of castrate-resistant prostate cancer patients using an antibody for prostate-specific membrane antigen (PSMA), a highly prostate specific cell-surface antigen. The approach they have followed is the use of staggered obstacle arrays to create size dependent particle trajectories that maximize PCTCobstacle wall interactions while minimizing the interactions of other blood cells. This technique was termed as geometrically enhanced differential immunocapture (GEDI). The GEDI device geometry was designed to maximize streamline distortion and thus bring desired cells in contact with the immunocoated obstacle walls for capture. Blood is a dense heterogeneous cell suspension consisting of cells of various sizes ranging from approximately 4 to 18 mm in size. PCTCs, in contrast, are larger and range from 15 to 25 mm in diameter. Relative obstacle alignment was chosen so that the displacement caused by cell impact with obstacles increases the likelihood of future cell impacts for large cells more than for small cells. Thus when cell-obstacle impact does not

lead to capture, larger cells are displaced onto streamlines that impinge onto the next obstacle, while smaller cells are displaced onto streamlines that do not impinge [8].

M. Toner et al developed a new concept which included the integration of vertically aligned carbon nanotubes (VACNTs) on the obstacle wall. To enhance the efficiency, they arranged the micro-post arrays perpendicular to the flow, spanning across the height of the channel. This improves cell-surface interactions by increasing the overall surface area, as well as by bringing capture surfaces closer to cells passing through the center of the channel. The micro-post array design is used in some of the most efficient microfluidic devices for rare cell isolation. Isolation efficiency is a function of the interception efficiency and the binding efficiency. They have studied the interception efficiency in the flow regime of a typical microfluidic system, and shown that the interception efficiency can greatly be improved by using nanoporous posts instead of solid posts [10].

1.2.2 Study of Fluid Flow on Cylinders

The computational predictions of the relevant hydrodynamical parameters of the flow of a viscous incompressible fluid past a swarm of porous particles at nanoscale are of considerable practical and theoretical interest of many physical, engineering, and medical problems. Deo et al have discussed an aggregate of porous nanocylindrical particles is considered as a hydro-dynamically equivalent to a solid cylindrical core with concentric porous cylindrical shell. The Brinkman equation inside the porous cylindrical shell and the Stokes equation outside the porous cylindrical shell in their stream function formulations were used. Explicit expressions for the stream functions in both regions were investigated. The drag force acting at each nanoporous cylindrical particle in a cell was evaluated. Also, they solved the same problem by using Happel boundary condition on the hypothetical cell. In certain limiting cases, drag force converges to pre-existing analytical results, such as the drag on a porous circular cylinder and the drag on a solid cylinder in Kuwabaras cell or Happels cell [22].

Srivastava discussed the uniform flow of an incompressible viscous fluid at small Reynolds number past a porous sphere of a radius with a solid concentric spherical core of a specific radius had been discussed. The region of the porous shell is called zone I which is fully saturated with the viscous fluid, and the flow in this zone is governed by the Brinkman equation. The space outside the shell where clear fluid flows is divided into two zones (II and III). In these zones the flow is discussed following Proudman and Pearsons method of expanding Stokes stream function in powers of Reynolds number and then matching Stokes solution with Oseens solution. The stream function of zone II is matched with that of zone I at the surface of the shell by the condition suggested by Ochoa Tapia and Whitaker [14].

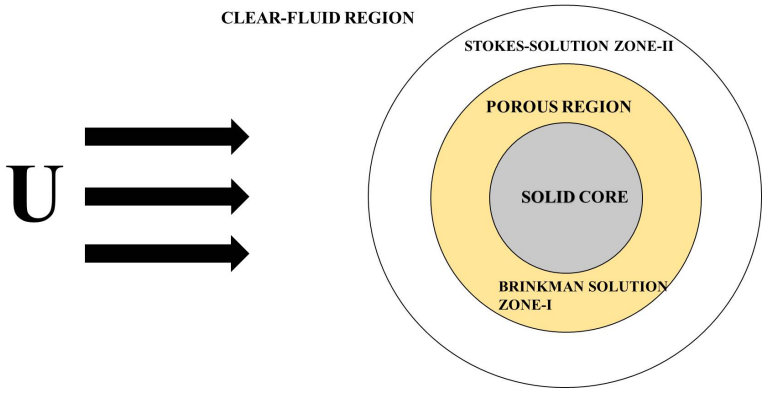

Figure 1.5. Fluid with velocity U that flows perpendicular to the axis of the cylinder. The cylinder is a composite cylinder that has a solid central core and a porous sheath covering. The Brinkman equation is solved in the porous region and the Navier-stokes in the fluid region [20].

Taamneh and Bataineh investigated axisymmetric viscous, two-dimensional steady and incompressible fluid flow past a solid sphere with porous shell at moderate Reynolds numbers. They have studied the Reynolds number based on the free stream fluid velocity and the diameter of the solid core, and the ratio of the porous shell thickness to the square root of its permeability. The flow in the free fluid region outside the shell is governed by the NavierStokes equation. The flow within the porous annulus region of the shell is governed by a Darcy model. In their study, parametric

equation relating the drag coefficient and separation point with the Reynolds number and porosity parameter were obtained by multiple linear regressions. In the limit of very high permeability, the computed drag coefficient as well as the separation angle approaches that for a solid sphere of radius a, as expected. In the limit of very low permeability, the computed total drag coefficient approaches that for a solid sphere of radius b, as expected. It was found that the total drag coefficient around the solid sphere as well as the separation angle is strongly governed by the porous shell permeability as well as the Reynolds number. The separation point shifts toward the rear stagnation point as the shell permeability is increased. Separation angle and drag coefficient for the special case of a solid sphere of radius $r = a$ was found to be in good agreement with previous experimental results and with the standard drag curve [13].

Noymer et al, speaks about the drag on a permeable cylinder in steady flow at moderate Reynolds numbers. There are two dimensionless parameters in their study are the Reynolds number based on the free-stream fluid velocity and the diameter of the cylinder, and the ratio of the permeability of the cylinder to the square of the cylinder diameter. In the limit of very low permeability, the computed drag coefficient approaches that for a solid cylinder, as expected. In the limit of very high permeability, the computed drag coefficient asymptotically approaches zero, a phenomenon that can be predicted using Darcy's Law. Between these extremes in permeability, a distinct dependence of the behavior of the computed drag coefficient on Reynolds number was observed. For higher Reynolds numbers, an increase in drag of up to 50% over that for a solid cylinder has been computed, while for lower Reynolds numbers, very little change in drag was observed. In the inner region, mass conservation and Darcy's law for flow in a permeable body are applied in order to solve for the pressure and velocity fields [20].

The mass conservation equation for two-dimensional, incompressible flow is given by the following expression

$$\bigtriangledown.\vec{V} = 0 \tag{1.1}$$

and the conservation of momentum is expressed in Darcy's Law:

$$\bigtriangledown P = 0 \tag{1.2}$$

A modification to Darcy's law established by Brinkman is a more general statement of momentum conservation. However, an order-of-magnitude analysis shows that Brinkman's formulation reduces to Eq.1.2 when the ratio of permeability and the square of the system length scale is less than unity. In subsequent sections, we define this ratio as the permeability ratio and in this study; the permeability ratios considered are generally orders of magnitude smaller than unity, or approaching unity in some cases. As a result, we believe that Eqs.1.1 and 1.2 adequately describe the flow field within the porous cylinder [18].

In the outer region, the mass conservation expression of Eq.1.1 is applied, while the steady-state, two dimensional, incompressible form of the Navier-Stokes equation is used to solve for the momentum of the fluid flow:

$$\rho\vec{V}.\bigtriangledown\vec{V} = -\bigtriangledown P + \mu\bigtriangledown^2\vec{V} \tag{1.3}$$

The solutions for the pressure and mass flow are matched at the interface of the two regions, and the boundary conditions that are specified are the pressure on the exterior of the domain and the velocity on the exterior of the domain to the windward side of the cylindrical body [20]. Matching the mass flow of the outer region to that of the inner region at the interface of the two regions provides the second boundary condition for velocity required by Eq.1.3.

Grosan and Pop have carried out an analytical investigation for a two-dimensional steady, viscous, and incompressible flow past a permeable sphere embedded in another porous medium using the Brinkman model, assuming a uniform shear flow far away from the sphere. Semi-analytical solutions of the problem were derived and relevant

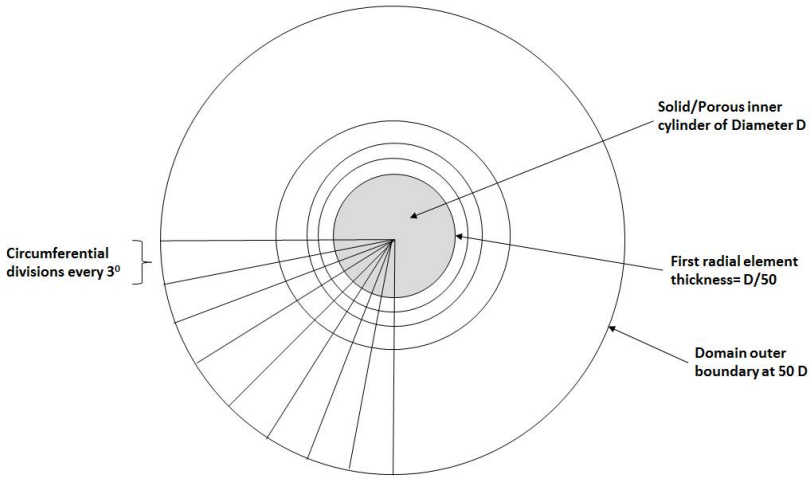

Figure 1.6. Cylinder consisting of a solid inner cylinder that is immersed in another porous medium [20].

quantities such as velocities and shearing stresses on the surface of the sphere are obtained. The streamlines inside and outside the sphere and the radial velocity are shown in several graphs for different values of the porous parameters. It was shown that the dimensionless shearing stress on the sphere is periodic in nature and its absolute value increases with an increase of both porous parameters [7].

1.3 Objectives of Present Research

The development of microchips for the separation of rare cells has been very impressive over the past few years. Table 1.1 summarizes the type of separation that has been used in previous studies and the principle of separation underlying it. It also includes the design that is contributed by the present work.

However, some drawbacks still exist. Few of the major shortcomings that lead to reduction in efficiency of the chip are low throughput and selectivity, lower cell capture efficiency, high shear stress at the walls of the posts, low interception efficiency etc.

Nagrath et al, utilized solid microposts for capturing CTCs. Though an efficient model, the use of solid microposts brought about some challenges such as high hydrodynamic resistance between the posts and the cells, thereby decreasing the interception efficiency. The widely used definition of interception efficiency is given by $\eta = \frac{b}{d_c}$, where b is the span of particles upstream that are ultimately intercepted by the collector, and d_c is the collector diameter [4, 10].

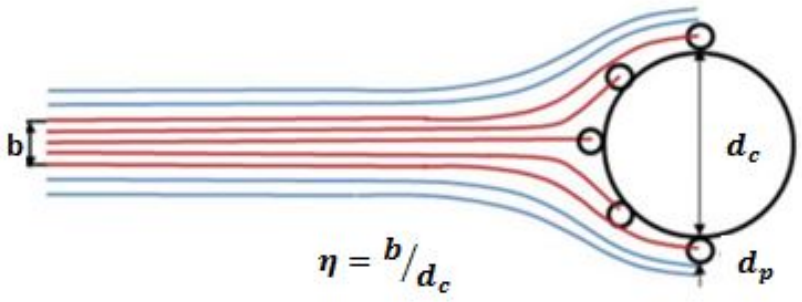

Figure 1.7. Deduction of efficiency of cell capture. b is the span of particles upstream. Higher b leads to higher capture efficiency [10].

The present research is directed towards five main objectives. The achieving of these goals would help us in increasing the capture efficiency.

The first objective is to achieve lower shear force on the cylindrical microposts by the fluid. By ensuring lower shear stress, the cells are more likely to come in contact with the posts and remain in contact with the post, thereby increasing the capture efficiency.

Secondly, from the definition of efficiency shown above, efficiency increases with the increase in the parameter b which is the span of particles upstream that are ultimately intercepted. The post diameter dc is taken to be constant throughout the study and hence the increase in bandwidth or span of the particles ultimately results in the increase in capture efficiency.

In order to achieve higher capture efficiency, the alternate design approach we proposed was to use a porous cylindrical shell with a solid impermeable core. The

study of this design and the parameters that would influence this flow would be our third objective.

A major influence on the capture efficiency is the arrangement of posts. Initially the study is carried out on an equilateral triangle arrangement and then with few modifications in the arrangement, it shown how the capture efficiency is enhanced. This will form the fourth objective of the study.

The fifth objective is to chemically coat the posts with nucleic acid aptamers. The advantages of coating the posts with these aptamers are that they increase the binding affinity and binding selectivity and also are relatively less toxic. Also they are small in size, easy to synthesize and are tolerant to harsh conditions. The surface of the posts is decorated with Silicon Nanopillars which serve as a binding or trapping medium of the rare cells. This is because of the Microvilli and Filopodia present on the cell surface. They play an important role in epithelial cell-cell contact. Due to coating of the surfaces with nucleic acid aptamers that are specific to the binding of this Microvilli and Filopodia via the silicon nanopillars on the post surface, a high cell capture efficiency can be recorded [15].

Table 1.1. Summary of devices used indicating their advantages and disadvantages.

S.No	Name of Device	Principle	Advantages/Disadvantages
1.	Geometrically Enhanced Differential Immunocapture (GEDI)	This is justified and may go to second line as well, neatly induce a size-dependent collision frequency and streamline distortion. [8]	Efficiency of 65%-70%.
2.	MagSweeper Device	Based on immunomagnetic separation [5].	Low purity and low yield
3.	Circulating Tumor Cell (CTC) Chip	Array of microposts that are made chemically functional [4].	Due to presence of solid microposts, efficiency is greatly reduced.
4.	Nanoporous microposts with forest of VACNT	Porous microposts that are made up of Vertically Aligned Carbon Nanotubes [10].	High capture efficiency but device reusability is low. VACNT cannot withstand high shear forces and may break off.
5.	Chaotic Micromixing Device	Local topographic interactions between the silicon nanopillar (SiNP) and cell surface [1].	Presence of SiNP helps withstand high shear force. Contact efficiency between forest and cell wall is low.
6.	Present work	Forest of SiNP coated with Nucleic acid grown on the micropost surface [15].	Can withstand high shear force, hence increases throughput and efficiency.

2. THEORETICAL BACKGROUND

2.1 Navier Stokes Equations

The Navier-Stokes equations are the fundamental partial differentials equations that describe the flow of incompressible fluids. The conservation of mass is given by

$$\frac{\partial \rho}{\partial t} + \bigtriangledown.(\rho \vec{V}) = 0 \tag{2.1}$$

$$\vec{V} = u\vec{i} + v\vec{j} \tag{2.2}$$

Because our primary unknowns are the flow properties (u, v, ρ, r, T) there is a need to link the stresses t with these physical variables. In solid mechanics (Hooke's law) stress is set proportional to strain. This works for solids because a solid undergoes only a finite amount of deformation when a force or stress is applied to it. In fluid mechanics, this approach does not work because fluid continuously deforms when a shear stress is applied. It is this characteristic that distinguishes a fluid from a solid [20].

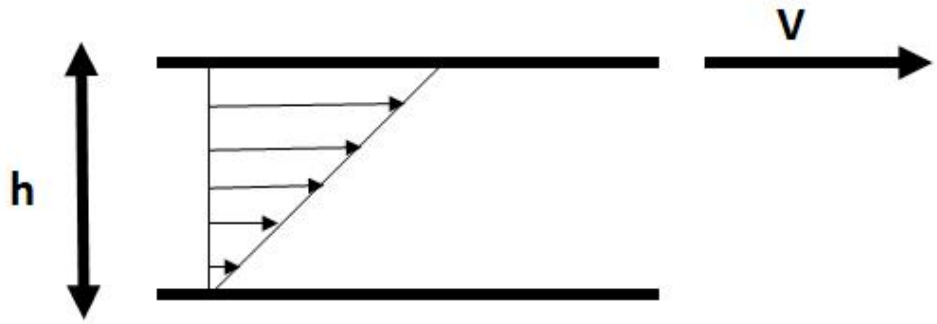

Figure 2.1. : Fluid that is contained between two parallel plates.

Newton came up with the idea of requiring the stress τ to be linearly proportional to the time rate at which strain occurs. Specifically he studied the following problem.

There are two flat plates separated by a distance $'h'$. The top plate is moved at a velocity $'V'$, while the bottom plate is held fixed. Newton postulated (since then experimentally verified) that the shear force or shear stress needed to deform the fluid was linearly proportional to the velocity gradient:

$$\tau = \frac{V}{h} \tag{2.3}$$

The proportionality factor turned out to be a constant at moderate temperatures, and was called the coefficient of viscosity, μ. Furthermore, for this particular case, the velocity profile is linear, giving $V/h = \partial u/\partial y$. Therefore, Newton postulated:

$$\tau = \mu \frac{\partial u}{\partial y} \tag{2.4}$$

Stokes Hypothesis:

Stokes extended Newton's idea from simple 1-D flows (where only one component of velocity is present) to multidimensional flows. Here, the fluid element may experience a strain rate both due to gradients such as $\partial u/\partial y$ as well as $\partial v/\partial x$. He developed the following relations, collectively known as Stokes relations.

$$\tau_{xx} = 2\mu \frac{\partial u}{\partial x} + \lambda(\frac{\partial u}{\partial x} + \frac{\partial v}{\partial y} + \frac{\partial w}{\partial z}) \tag{2.5}$$

$$\tau_{yy} = 2\mu \frac{\partial v}{\partial y} + \lambda(\frac{\partial u}{\partial x} + \frac{\partial v}{\partial y} + \frac{\partial w}{\partial z}) \tag{2.6}$$

$$\tau_{zz} = 2\mu \frac{\partial w}{\partial z} + \lambda(\frac{\partial u}{\partial x} + \frac{\partial v}{\partial y} + \frac{\partial w}{\partial z}) \tag{2.7}$$

$$\tau_{xy} = \tau_{yx} = \mu(\frac{\partial u}{\partial y} + \frac{\partial v}{\partial x}) \tag{2.8}$$

$$\tau_{yz} = \tau_{zy} = \mu(\frac{\partial w}{\partial y} + \frac{\partial v}{\partial z}) \tag{2.9}$$

$$\tau_{xz} = \tau_{zx} = \mu(\frac{\partial u}{\partial z} + \frac{\partial w}{\partial x}) \tag{2.10}$$

For 2-D flows, somewhat simpler expressions are obtained if we set w, the z-component of velocity, to zero, and if we set all derivatives with respect to z to be zero.

The conservation of momentum in the x-direction is given by

$$\frac{\partial(\rho u)}{\partial t} + \frac{\partial(\rho u^2 + p)}{\partial x} + \frac{\partial(\rho uv)}{\partial y} = \frac{\partial \tau_{xx}}{\partial x} + \frac{\partial \tau_{xy}}{\partial y} \tag{2.11}$$

And in the y-direction is given by

$$\frac{\partial(\rho v)}{\partial t} + \frac{\partial(\rho v^2 + p)}{\partial y} + \frac{\partial(\rho uv)}{\partial x} = \frac{\partial \tau_{yy}}{\partial y} + \frac{\partial \tau_{xy}}{\partial x} \tag{2.12}$$

2.2 Darcy's Law: Porosity and Permeability

The fluid storage capacity of porous media is mainly determined by its porosity, whereas the absorption and spreading rate is determined by the permeability. The permeability coefficient may be calculated by Darcy's Equation [18].

Permeability is the most important physical property of a porous medium, while the porosity is its most important geometrical property. The permeability describes the conductivity of a porous medium with respect to fluid flow, whereas the porosity is a measure of the fluid storage capacity of a porous material. Permeability describes how easily a fluid is able to move through the porous material. It is calculated using a formula known as Darcy's Law.

Current equations describing fluid transport in porous media are based on semi-empirical equations derived in the 19th century by Darcy for single-phase flow and in the 20th century for multiphase flow. These equations describe the average behavior of a mixture of a porous medium and one or more fluids. Darcy's law describes the kinetics of fluid flow through porous media in terms of the driving force and the permeability of the medium.

Darcy's law is defined by

$$Q = \frac{K}{\eta}\frac{\Delta P}{\Delta L}A \tag{2.13}$$

Q =Flow rate (m^3/s)

K =Permeability coefficient (m^2)

ΔP =Pressure drop or difference

L =Flow length or thickness of test sample (m)

A =Area of cross-section (m^2)

η =Fluid viscosity $(Pa.s)$

The permeability coefficient K depends on the combination of fluid and porous material used. The greater the value of K, the higher will be the rate of flow of a fluid through material.

2.3 Brinkman Equations for Flow Past Porous Cylinders

When a unidirectional flow encounters a porous cylinder, a complex field develops partially through and partially around the cylinder. The prediction of the flow rate passing through and flowing around the cylinder is not straight forward and depends on many factors such as the physical properties of the medium in question. The present section focuses on the problem of flow and concentration distribution around and through a porous cylinder for low and moderate Reynolds number range for non-potential flows [11, 14, 18].

Regions with the smaller pores are treated as a permeable medium and flow is described by Darcy's law. The two boundary conditions to be satisfied at the pore/permeable medium interface are continuity of the fluid velocity and the shear stress. Darcy's law alone is not sufficient to satisfy these boundary conditions. The Brinkman equation is a generalization of Darcy's law that facilitates the matching

of boundary conditions at an interface between the larger pores and the permeable medium.

Brinkman's equation is

$$\bigtriangledown P = -\frac{\mu}{K}\vec{V} + \mu_e \bigtriangledown^2 \vec{V} \tag{2.14}$$

We consider a long cylinder of radius a placed in a uniform flow (from left to right) with velocity U. A two-dimensional, laminar, incompressible and steady flow of a fluid with constant properties is considered. We take the characteristic length as a and characteristic velocity U with center of the cylinder as origin in polar co-ordinates (r,θ) and the initial line along the direction of the uniform stream. The single set of equations in non-dimensional form is presented. The radial coordinate r is measured from the center of the cylinder while the angular coordinate (θ) is measured from the forward stagnation point of the cylinder.

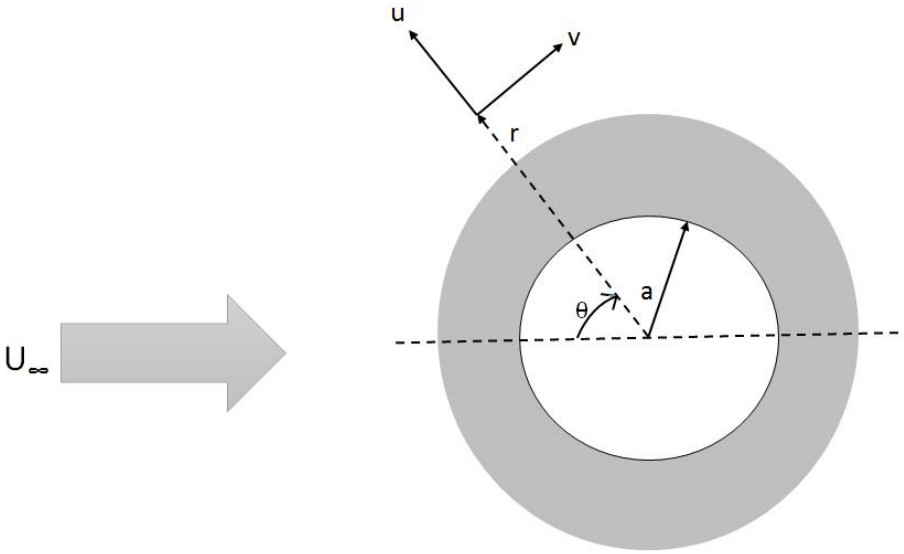

Figure 2.2. Representation of the flow of fluid perpendicular to the axis of the cylinder in polar coordinates.

The dimensionless continuity equation in terms of Darcy velocities are

$$\frac{\partial}{\partial r}(ru) + \frac{v}{\theta} = 0 \tag{2.15}$$

The continuity and Brinkman equations, with inertial terms omitted are given by

$$\bigtriangledown.\vec{V} = 0 \tag{2.16}$$

$$\bigtriangledown P = -\frac{\mu}{K}\vec{V} + \mu_e \bigtriangledown^2 \vec{V} \tag{2.17}$$

The dimensionless momentum equations based on the Brinkman model are

$$-\frac{\partial p}{\partial r} = u - \sigma^2(\frac{\partial^2 u}{\partial r^2} + \frac{1}{r}\frac{\partial u}{\partial r} + \frac{1}{r^2}\frac{\partial^2 u}{\partial \theta^2} - \frac{u}{r^2} - \frac{2}{r^2}\frac{\partial v}{\partial \theta}) \tag{2.18}$$

$$-\frac{1}{r}\frac{\partial p}{\partial \theta} = v - \sigma^2(\frac{\partial^2 v}{\partial r^2} + \frac{1}{r}\frac{\partial v}{\partial r} + \frac{1}{r^2}\frac{\partial^2 v}{\partial \theta^2} - \frac{v}{r^2} + \frac{2}{r^2}\frac{\partial v}{\partial \theta}) \tag{2.19}$$

where

$$p = \frac{\mu p^\star}{aKu^\star_\infty} \tag{2.20}$$

The permeability K is related to the porosity φ by

$$K = \frac{d^2\varphi^3}{A(1-\varphi)^2} \tag{2.21}$$

where A is the Ergun constant and d is the particle diameter. This is known as the Kozeny Carman equation. The quantity σ is a small dimensionless parameter defined as

$$\sigma = \frac{1}{a}\sqrt{\frac{K}{\varphi}} \tag{2.22}$$

Introducing the stream function ψ such that

$$u = -\frac{1}{r}\frac{\partial \psi}{\partial \theta} \tag{2.23}$$

$$v = \frac{\partial \psi}{\partial r} \tag{2.24}$$

so that the continuity equation is satisfied. Eliminating p from equations, the dimensionless momentum equations reduce to

$$\sigma^2 \nabla^4 \psi - \nabla^2 \psi = 0 \tag{2.25}$$

$$\nabla^2 = \frac{\partial^2}{\partial^2} + \frac{1}{r}\frac{\partial}{\partial r} + \frac{1}{r^2}\frac{\partial^2}{\partial \theta^2} \tag{2.26}$$

The boundary conditions on the wall of the cylinder are such that there is no velocity slip, therefore,

$$\psi(r, \theta) = \frac{\partial \psi}{\partial r}(r, \theta) = 0$$

at

$$r = 1 \tag{2.27}$$

2.4 Darcy-Brinkman Equation for Flow through an Array of Cylinders

In most of those studies, the flow field inside the, porous bodies is described by the Darcy equation and the NavierStokes equations are used usually under creeping flow conditions to model the flow outside the body. This approach requires an appropriate boundary condition at the interface of the porous body. However, in many applications non-Darcian effects including shear and non-linear effects within the porous matrix and the viscous effects at the interface become significant under various conditions. Hence, for the extension of the Darcy equation, the Brinkman equation is used. The Darcy-Brinkman equation is a governing equation for flow through a porous medium with an extra Laplacian (viscous) term (Brinkman term) added to the classical Darcy equation. The equation has been used widely to analyze high-porosity porous media. The dynamic viscosity, μ_e, associated with the Brinkman

term is referred to as the effective viscosity. Studies in the past yielded varying results for the magnitude of the viscosity ratio $\hat{\mu}$ between slightly less than unity to as high as $< \sim 10$ for high porosity porous media [26, 27].

It is given by

$$\hat{\mu} = \frac{\mu}{\mu_e} \tag{2.28}$$

In the present section our subject of interest is flow over regular arrays of circular cylinders. The analysis which solves the Navier- Stokes equations rather than the Darcy equation, yields a relation between the permeability of the regular array structure and the porosity (volume fraction occupied by the flow), confirming that the Darcy equation is valid for flow through regular structures over the whole spectrum of the porosity. Therefore, quantitative relations between the wall effects and the Darcy-Brinkman equation may be examined in a more focused manner. The Darcy-Brinkman equation in recent years is employed in biomedical hydrodynamic studies, including its use in modeling a thin fibrous surface layer coating blood vessels (endothelial surface layer) as it is a highly permeable, high porosity porous medium. A better understanding of the characteristics of the Darcy-Brinkman equation, therefore, is an important part of more practical problems.

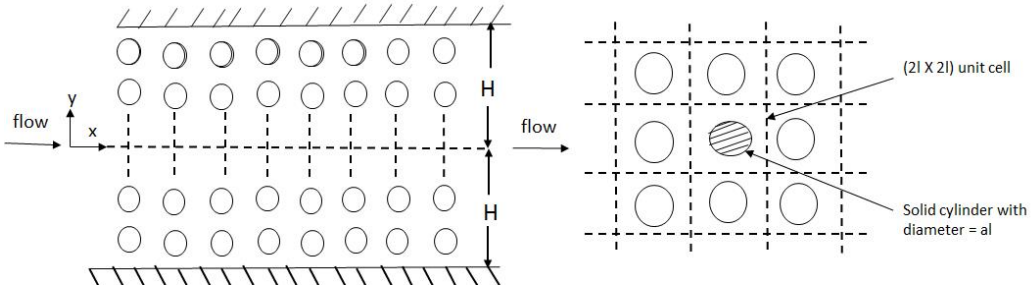

Figure 2.3. (a) Flow between two parallel plates filled with regular square arrays of circular cylinders,(b) Regular square arrays of circular cylinders.

As shown in the Fig. 2.3, we consider a steady, incompressible, fully-developed, and very slow (Re $\rightarrow$ 0, Creeping flow) flow across regular square arrays of circular

cylinders, bounded by parallel plates. Governing equations based on the Darcy-Brinkman equation for porous media and the boundary conditions are,

$$\frac{dp}{dx} = -\frac{\mu}{K}u_s + \mu_e\frac{d^2u}{dy^2}, u(y=H) = 0, \frac{du}{dy}(y=0) = 0 \tag{2.29}$$

In terms of non-dimensional variables defined as, $\tilde{y} = \frac{y}{H}$, $\tilde{u} = \frac{u}{u_m}$,$u_m = q/2H$

$$\frac{H^2}{\mu_e u_m}(-\frac{dp}{dx}) = \frac{1}{\hat{mu}}\frac{H^2}{K}\tilde{u} - \frac{d^2\tilde{u}}{d\tilde{y}^2}, \tilde{u}(\tilde{y}=1) = 0, \frac{d\tilde{u}}{d\tilde{y}}(\tilde{y}=0) = 0 \tag{2.30}$$

The formulation and its solution become,

$$\tilde{u} = \frac{K}{\mu u_m}(-\frac{dp}{dx})[1 - \frac{\cosh(Da.\frac{\tilde{y}}{\sqrt{\hat{\mu}}})}{\cosh(\frac{Da}{\hat{\mu}})} \tag{2.31}$$

where, $\hat{\mu} = \frac{\mu}{\mu_e}$, $Da = H/\sqrt{K}$

Upon an integration of the governing equation, over the channel half-depth, H, $\int_0^1 \tilde{u}d\tilde{y} = 1 = \int_0^H udy/H$ we obtain the following equation for the pressure gradient:

$$\frac{H^2}{\mu_e u_m}(-\frac{dp}{dx}) = \frac{Da^2}{1 - \frac{\tanh(\frac{Da}{\sqrt{\hat{\mu}}})}{Da/\sqrt{\hat{u}}}} \tag{2.32}$$

Since $\lim_{x\to 0}\tanh x \approx x - \frac{x^3}{3}$ the viscous flow limit is reached as $K \to \infty, Da \to 0$,

$$\frac{H^2}{\mu_e u_m}(-\frac{dp}{dx})_{ViscousLimit} = 3\hat{\mu} \tag{2.33}$$

The viscous flow limit corresponds to the case of $\hat{\mu} = 1$ in the equation above. The Darcian limit of flow through a porous medium is recovered as $K \to 0, Da \to \infty$

$$\frac{H^2}{\mu_e u_m}(-\frac{dp}{dx})_{DarcianLimit} = \frac{H^2}{K} = Da^2 \tag{2.34}$$

For the case of our interest, the porous medium consisting of regular square arrays of cylinders, the permeability, K , may be expressed as

$$K = \frac{(2l)^2}{f(C)} \Rightarrow Da = \sqrt{f(C)}.(\frac{H}{2l} \tag{2.35}$$

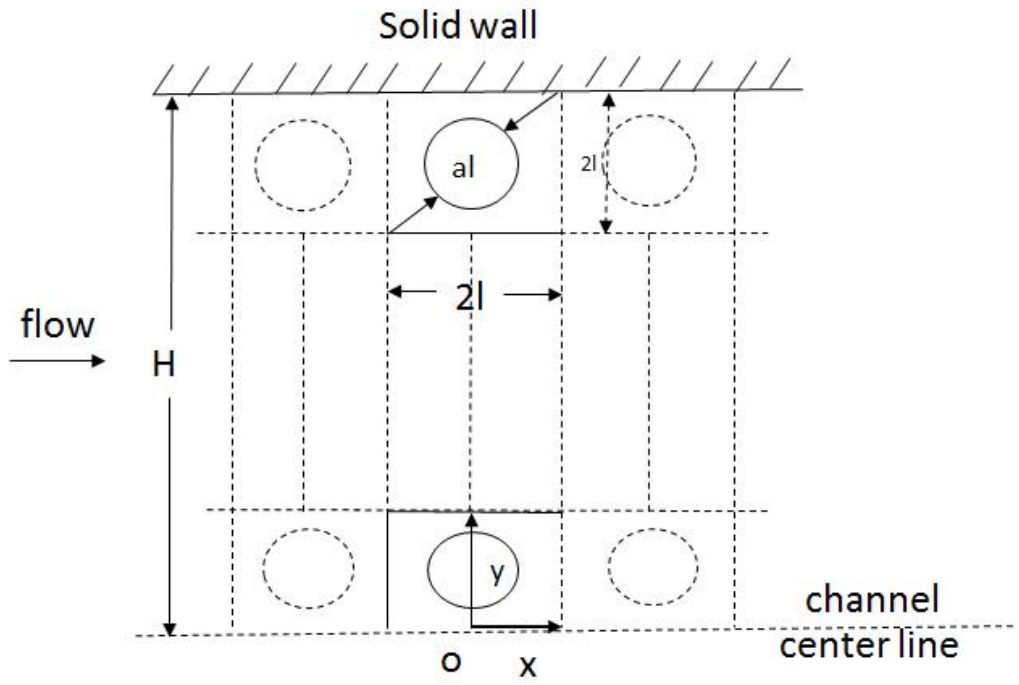

Figure 2.4. The porous medium consisting of regular square arrays of cylinders

where C(solid fraction) $= 1 - \varphi$, $\varphi = porosity, 2l =$ side length of a single square unit.

Referring to the Fig. 2.3, governing equations and boundary conditions are

$$\nabla.\vec{V} = 0, 0 = -\nabla p + \mu\nabla^2\vec{V}$$

with

$$\vec{V} = u\vec{i} + v\vec{j} \tag{2.36}$$

$$u = v = 0at(x, y) = (-l \leq x \leq l, y = H) \tag{2.37}$$

and on cylinder surface

$$\frac{\partial u}{\partial x} = 0at(x, y) = (\pm l, 0 \leq y \leq H), \tag{2.38}$$

$$\frac{\partial u}{\partial y} = v = 0at(x, y) = (-l \leq x \leq l, y = 0) \tag{2.39}$$

2.5 Capture and Interception Efficiency

A number of theoretical and experimental studies exist on particle interception across scientific disciplines ranging from aerosol science to marine ecology. The widely used definition of interception efficiency is given by $\eta = \frac{b}{d_c}$, where b is the span of particles upstream that are ultimately intercepted by the collector, and d_c is the collector diameter [10].

There are four classical mechanisms for interception: direct interception, diffusion, inertial compaction, and gravitational sedimentation. Contribution from each mechanism is additive to the overall efficiency. Direct interception occurs when a particle of a finite size travels along a streamline that approaches a collector by a distance less than the particle radius. The particle is brought directly into contact with the collector by the fluid streamline.

For creeping flows, the interception efficiency due to direct interception has been analytically solved as

$$\eta = A_F(\frac{d_p}{d_c})^2 \tag{2.40}$$

where d_p denotes particle diameter and

$$A_F = (2 - \ln\frac{2d_cU}{\nu})^{-1} \tag{2.41}$$

where U denotes average flow velocity and ν denotes the kinematic viscosity for isolated cylinders, and

$$A_F = (-\ln\alpha - \frac{3}{2} + 2\alpha - \frac{\alpha^2}{2})^{-1} \tag{2.42}$$

for cylinder arrays with volume fraction α.

Brownian diffusion of small particles in a fluid can cause them to randomly cross streamlines, increasing their probability of getting intercepted by the collector. This probability is greatly enhanced as their diffusive activity increases, due to increases in temperature, small particle size, or long residence time in proximity to the collector.

The contribution of Brownian diffusion as a mechanism of interception is additive with the effect due to direct interception, and is derived for a cylindrical collector as

$$\eta_{diff} = \frac{3.64 A_F}{Pe^{2/3}} \tag{2.43}$$

where Pe is the Peclet number (convection/diffusion) given by LU/D, where L is the characteristic length, U is the average velocity, and $D = kT/6p\mu a_p$ is the diffusion coefficient.

3. OPTIMIZATION OF DESIGN PARAMETERS

Blood is dominated numerically and volumetrically by erythrocytes, thrombocytes, and leukocytes. Table 3.1 lists the sizes of the cells. Although blood cell populations have reasonably tight size distributions, rare cells often have widely variable and dynamic sizes, such as progenitor cells, fetal cells, and circulating tumor cells (CTCs). Size alone is insufficient to identify rare cells, but provides a distinguishing characteristic that allows for an increased interception between the cell and the micropost.

Table 3.1. Sizes of different types of cells that constitute the blood.

Cell type	Size (diameter)
Erythrocytes	6-9 μm
Thrombocytes	2-3 μm
Leukocytes	8-14 μm
Rare cells (CTCs)	15-25 μm

Several parameters assist in controlling the fluid flow through the chip. The dependence and optimization of such parameters will be the focus in this present chapter. Previously proved models will be discussed and additional new approach to this technology will be presented. The design parameters for this new model will be emphasized and optimizing these parameters to improve the capture efficiency, throughput and purity and thus will form the motive of the research.

The flow was considered as a steady flow and the full Navier-Stokes equation was used to carry out all the simulations and find solutions. This is to account for any inertial forces that may exist due to the presence of the Reynolds number term that is associated with the convective term in the Navier-Stokes equation. However,

after preliminary test simulations, the full Navier-Stokes equations and the simplified stokes equations were applied, it was observed that there was no difference in the overall capture efficiency and computational time. Thereby we could conclude that indeed $Re \ll 1$ holds true.

COMSOL Multiphysics v4.2a was used to simulate results for optimizing various flow parameters. The contribution to this field of research is the introduction of the solid cylinder with a porous shell. A comprehensive study is carried out to optimize the design parameters such that the capture efficiency and throughput is increased. A comparison is made between solid microposts and porous posts. Near a straight, nonpermeable wall, flow is parallel to the wall and motion along a streamline does not carry a cell to the wall. To bring cells in contact to a wall, we must either (i) depend on a diffusive process to cause cells to randomly move transverse to streamlines, (ii) apply a body force to move the cells transverse to streamlines, (iii) create geometries in the flow so that flow is accelerated, streamlines are compressed and the cells are effectively brought in proximity to the wall by motion along a streamline, or (iv) make the wall permeable and allow the streamlines to cross the interface. The major contributions to the flow specifically for the solid core with porous shell design is effect of Darcy number, reduction in drag and shear force, inlet velocity and arrangement of posts.

There have been results quantifying the same effects for solid and porous posts. These results will be used as a standard to compare the results produced in this study. A specific design for the number of posts and chip size is set. This set standard is derived from previous studies. The procedure to formulate results is by keeping some parameters constant and varying the others to see the effect of variation. The standard procedure would be to design a chip with dimensions of $1450 \times 600 \mu m$ consisting of 36 microposts. The design that is initially used is derived from previous studies. The cylindrical posts have a constant diameter of 100 μm. The posts are arranged such that they are at a distance of 50 μm from each other and form an equilateral triangle. Fig. 3.1 illustrates the initial design setup.

A constant inlet velocity of 500 $\mu m/s$ will be set except for when observing the effect of velocity. As seen from Table 3.1, we can safely assume the particle or cell size to be 18 μm. If the particle size is bigger, there is a better susceptibility of capturing it. To prove the ability of the chip to reach higher efficiency, we have chosen a particle or cell size that not only lies within the size range of rare cells but also is closer to the lower range of cell size. Therefore if the chip is optimized to have a high efficiency for a smaller cell size, then we can imply that the chip will render higher efficiency for larger cell sizes. To reduce the complexity of the flow, we are assuming the blood to be behaving as a Newtonian fluid. The properties of the fluid will be comparable to that of water with density being 1000 kg/m^3 and dynamic viscosity of 0.001 $Pa.s$. This similarity can be used by assuming that the blood is much diluted.

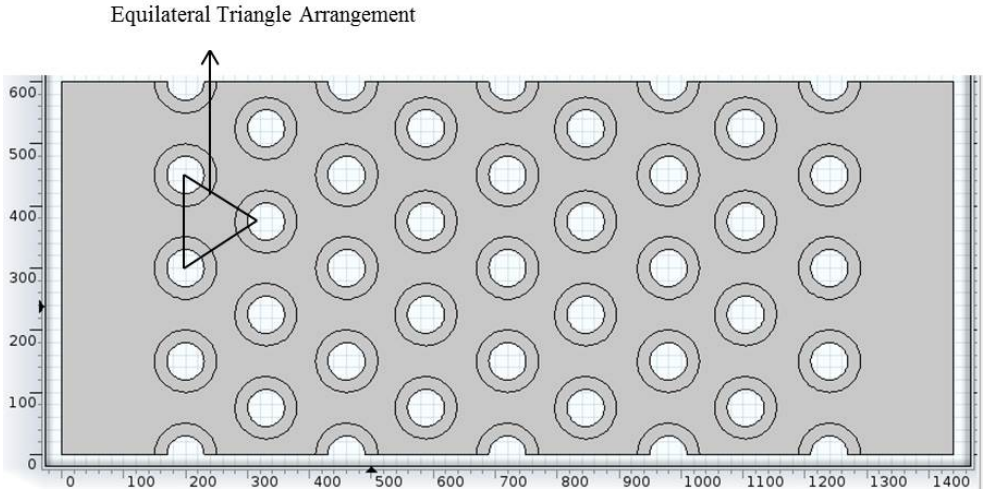

Figure 3.1. The equilateral triangle arrangement; all the posts are at an equal distance of 50 μm from each other.

3.1 Dependency of Capture Efficiency on Core to Shell Ratio

Cell transport toward solid boundaries is inherently limited by the no-penetration velocity condition at the boundarys surface; streamlines near the boundary run parallel to it. One simple solution to enhance motion normal to the surface is to use

porous walls combined with a transverse pressure gradient. This results in target particles being pulled toward the wall as the carrier fluid flows out of the channel. Unlike porous filter-based microdevices, particles are not trapped, but adhesion can be enhanced by direct contact and a pressure-induced normal force.

The design of the post is studied and adjusted according to the solid core radius to the constant post diameter of 100 μm. This means that the thickness of the porous shell surrounding the solid core is varied. The porous annulus region is varied from zero thickness to full post diameter. When the porous shell thickness is zero, then the posts are fully solid and when the shell thickness is maximum i.e. equal to the diameter of the post, the posts are fully porous. A study is carried out by varying this thickness and keeping the fabrication limitations in mind an appropriate ratio is chosen.

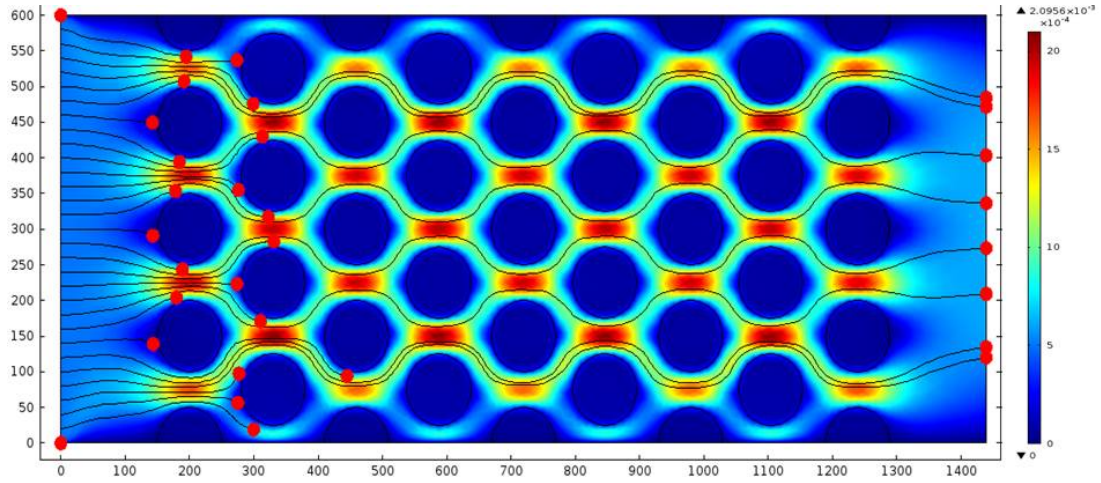

Figure 3.2. The number of particles captured for completely porous posts i.e. the solid core is absent ($a = 0$)

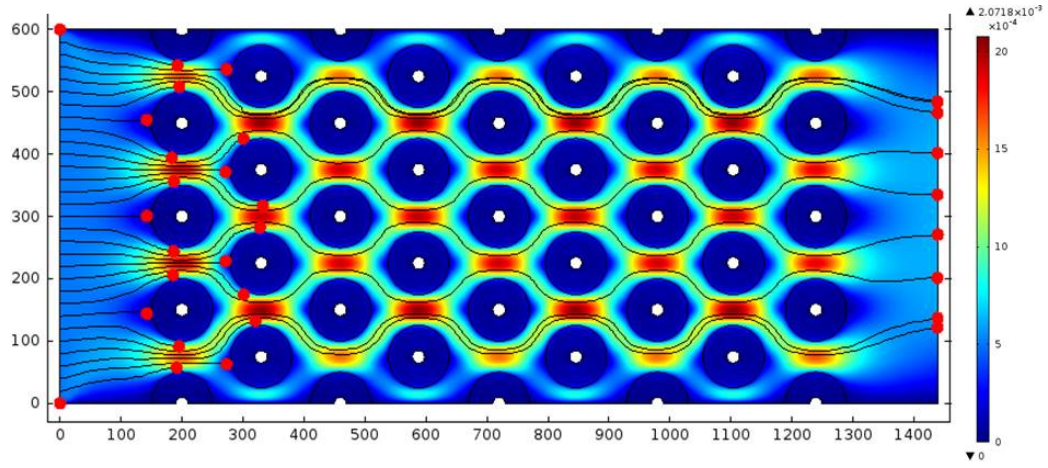

Figure 3.3. The number of particles captured for posts that have a core radius of 10 μm ($a = 10\ \mu m$)

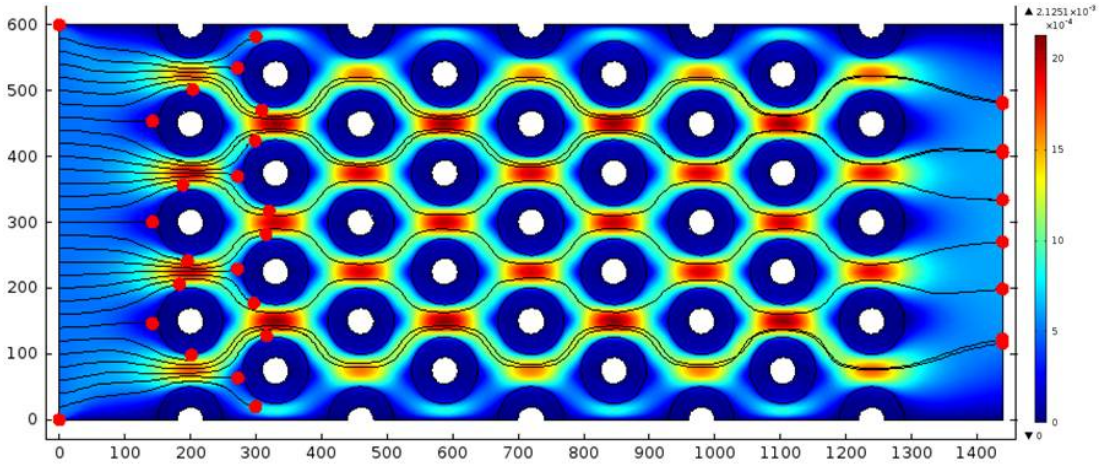

Figure 3.4. The number of particles captured for posts that have a core radius of 20 μm ($a = 20\ \mu m$)

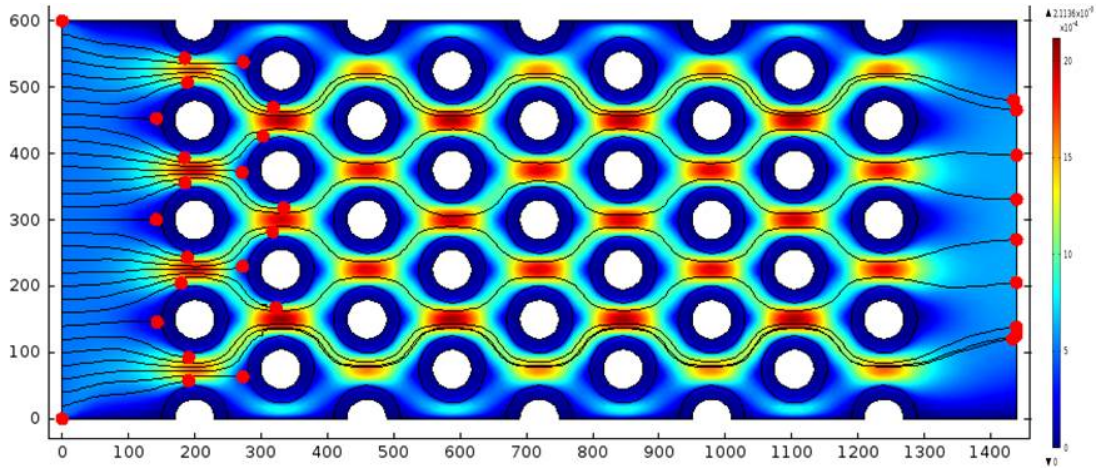

Figure 3.5. The number of particles captured for posts that have a core radius of 30 μm ($a = 30\ \mu m$)

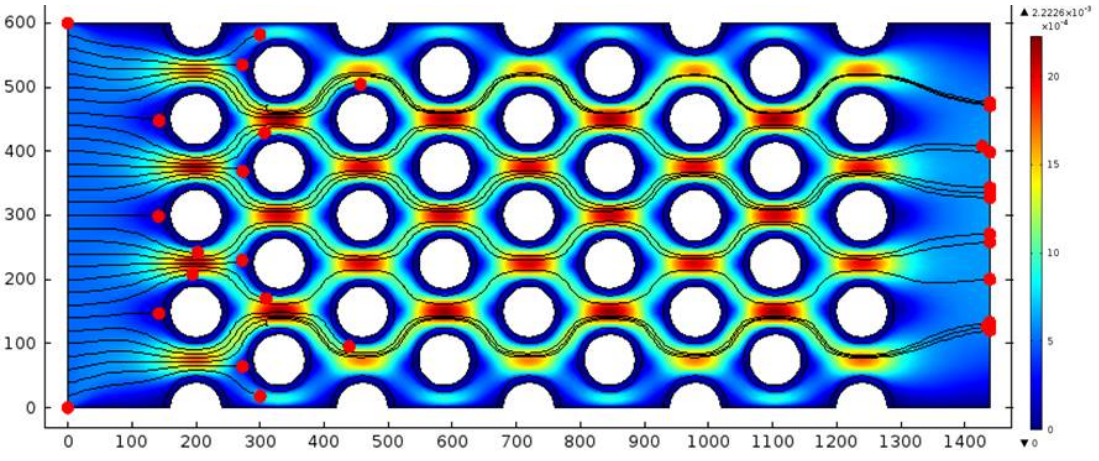

Figure 3.6. The number of particles captured for posts that have a core radius of 40 μm ($a = 40\ \mu m$)

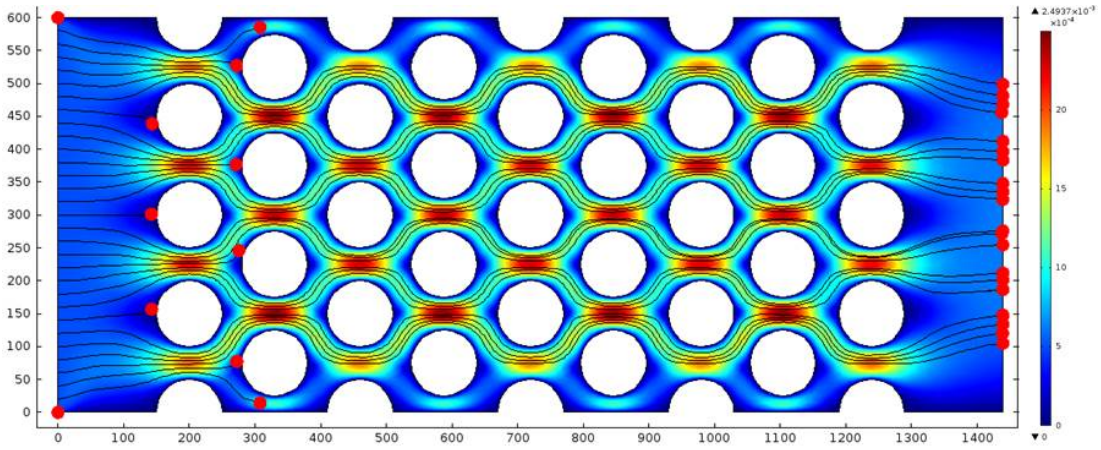

Figure 3.7. The number of particles captured for posts that are completely solid and have no porous sheath covering i.e. have a core radius of 50 μm ($a = 50\ \mu m$)

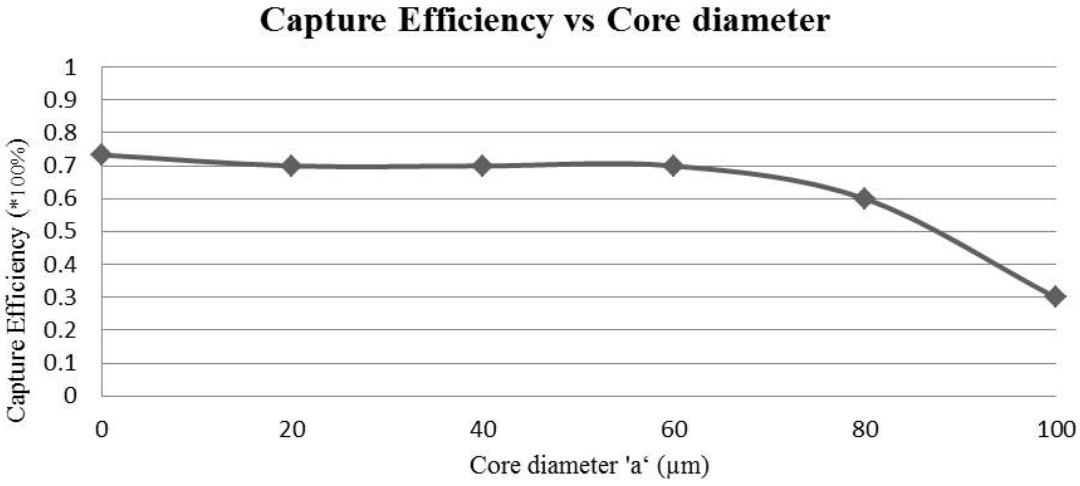

Figure 3.8. The change in capture efficiency with the increase in thickness of the porous layer around the cylinder.

From Fig. 3.8 it can be seen that the capture efficiency is highest for fully porous posts as expected because more amount of fluid can be passed through such posts. The curve for capture efficiency gradually decreases with the increase in solid core diameter. As the posts become fully solid i.e. $a = 0$, the capture efficiency is the least due to higher hydrodynamic resistance and higher shear forces. Therefore in order to achieve decent capture efficiency an optimum solid core diameter is chosen. Taking into account the fabrication limitations of designing a small core cylinder, a viable solid core diameter of 60 m is chosen for the study. Hence from here on, a constant b/a ratio of 1.67 is utilized. b is the post diameter which remains constant of 100 μm and a is the diameter of the solid core as shown in Fig. 3.9.

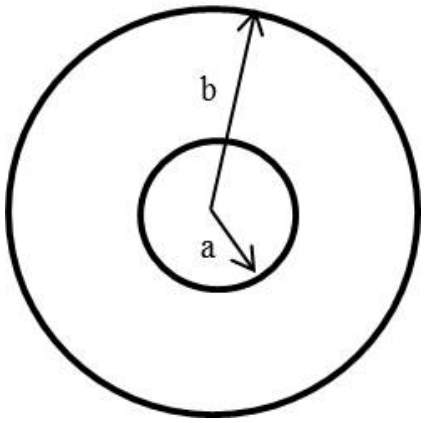

Figure 3.9. The change in capture efficiency with the increase in thickness of the porous layer around the cylinder.

3.2 Effect of Darcy Number on Capture Efficiency

Previous models have shown that the degree of fluid accessibility inside a porous post is related to its Darcy number, defined as $Da = K/{d_c}^2$, where K is the permeability of the porous material, and dc is the characteristic length, or the post diameter. The post diameter is kept constant to 100 μm in our study. Hence to vary the Darcy number, we varied the permeability and kept a constant porosity of 70%.

As the permeability (K) is decreased i.e. decreasing the Darcy number (Da) the overall capture efficiency decreases as less amount of fluid is allowed to pass through the porous shell and hence the susceptibility of the cells to come in contact with the posts is decreased. We have varied the Darcy number from 10^2 to 10^{-5}.

$K = 1 \times 10^{-6} m^2, Da = 10^2$

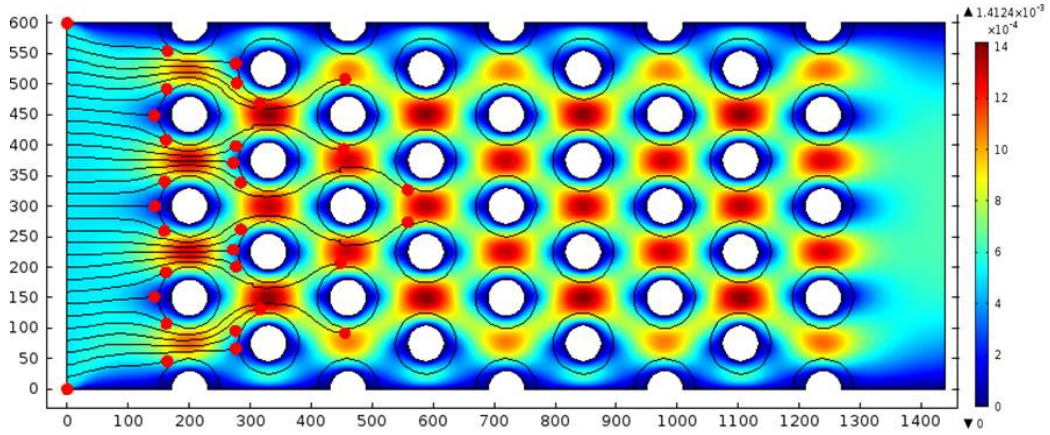

Figure 3.10. The number of particles captured when $Da = 10^2$. It is noticed that almost all the cells are captured. This is because of the high permeability K.

$K = 1.08 \times 10^{-9} m^2, Da = 0.108$

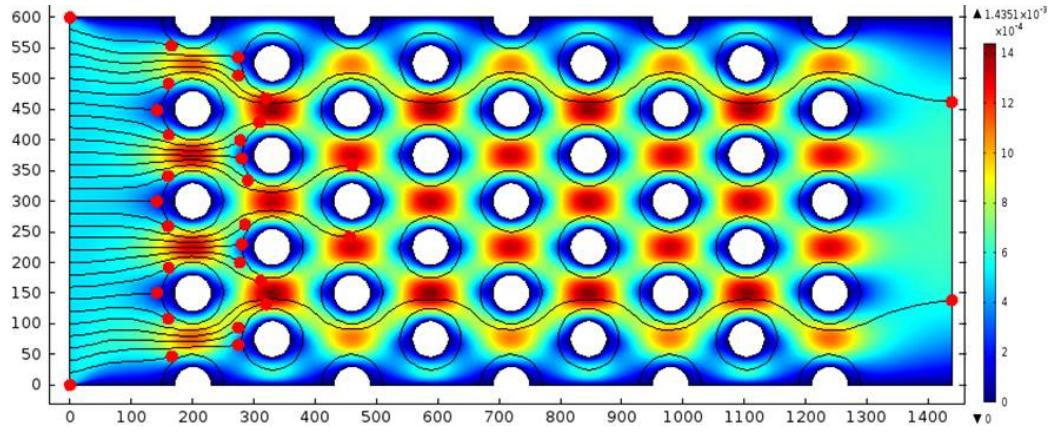

Figure 3.11. The number of particles captured when $Da = 0.108$. Due to the reduction in permeability K, fewer particles as compared to the previous case are captured.

$K = 1 \times 10^{-11} m^2, Da = 0.001$

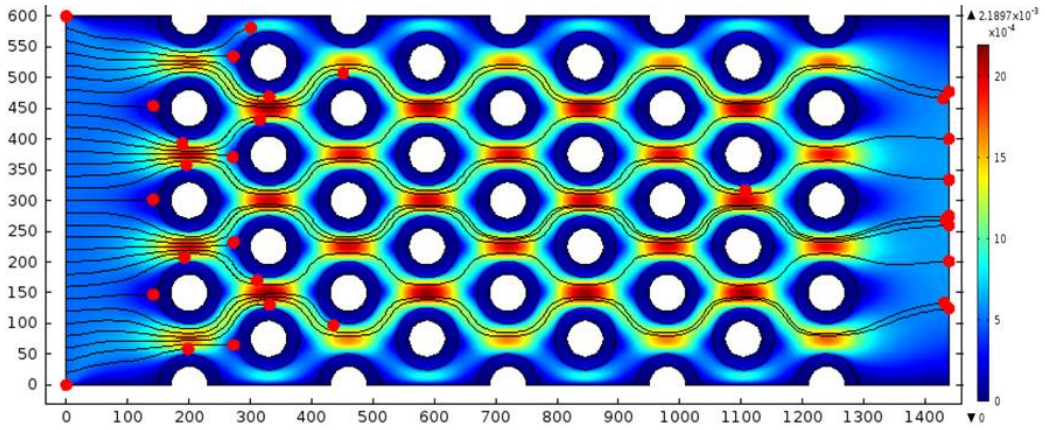

Figure 3.12. The number of particles captured when $Da = 0.001$. Due to the reduction in permeability K, fewer particles as compared to the previous case are captured.

$K = 5.1 \times 10^{-12} m^2, Da = 0.00051$

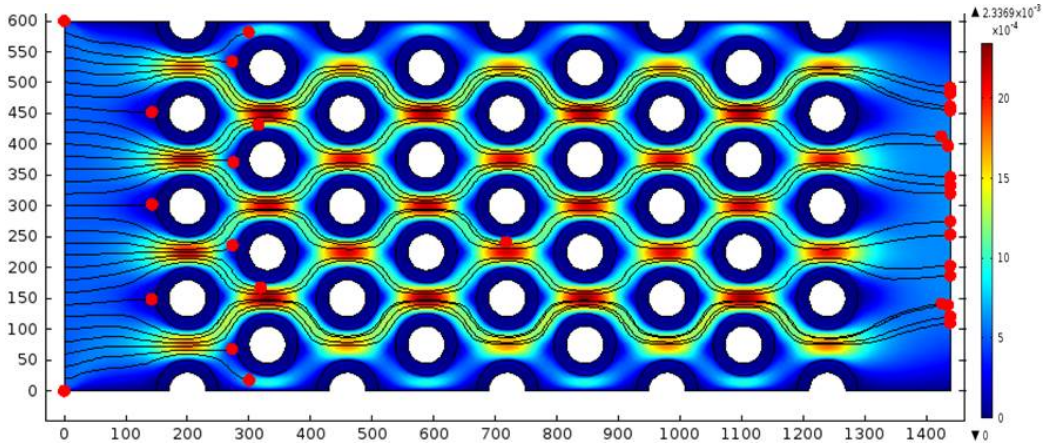

Figure 3.13. The number of particles captured when $Da = 0.00051$. Due to the reduction in permeability K, fewer particles as compared to the previous case are captured.

$K = 1 \times 10^{-13} m^2, Da = 10^{-5}$

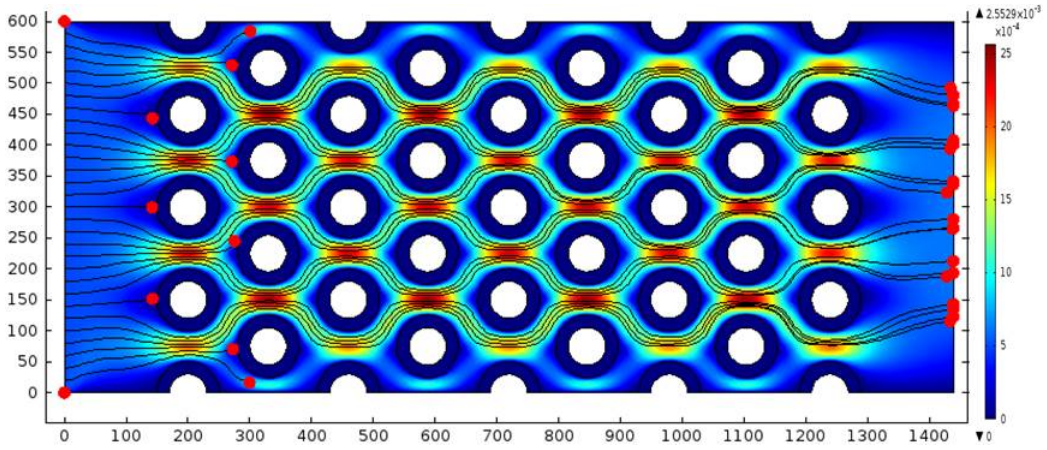

Figure 3.14. The number of particles captured when $Da = 10^{-5}$. Due to the reduction in permeability K, fewer particles as compared to the previous case are captured.

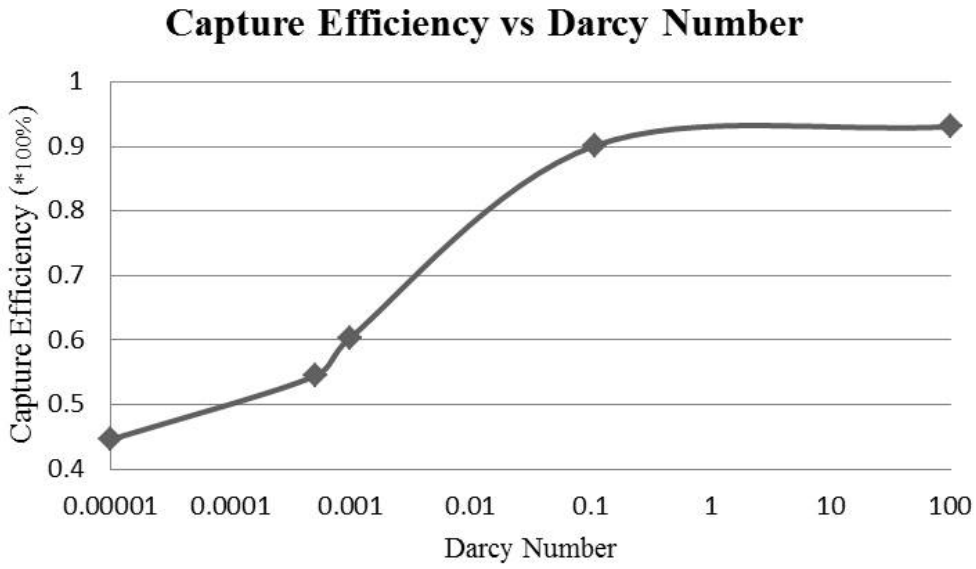

Figure 3.15. Behavior of capture efficiency when the Darcy number is varied.

This section shows the variation of the capture efficiency with the Darcy number. As the Darcy number is dependent on the permeability K, reduction in permeability

will lead to lower Darcy number and hence lower capture efficiency. The permeability is dependent on the density of the silicon nanowires that are present on the surface of the micro posts. Therefore, from previously accepted experimental observations, the permeability K we have chosen for the entire study henceforth is $1 \times 10^{-11} m^2$. This is an acceptable value as the capture efficiency is around 65% and we will later show that even with this value of permeability, we can achieve higher capture efficiency by modifying other parameters.

3.3 Variation of Capture Efficiency due to Drag and Shear stress

The Brinkman equation has the advantage that it contains the stress tensor, thus the boundary condition is the continuity assumption of momentum and viscous stress along the poroussolid interface boundary. Nazar et al. studied the boundary layer flow past a circular cylinder in a porous medium through the Brinkman model. Khanafer et al. employed the extended BrinkmanDarcy law to describe the flow motion inside the porous sleeve.

The local shear stress in a microfluidic device is a function of the device geometry, flow rate, and fluid properties. Both the maximum shear stress and the shear stress gradient can significantly impact viability as a cell traverses the device. Shear induced damage to cells simultaneously diminishes the population to be sampled and also contaminates any immunocoated surfaces with cell fragments. Therefore, the shear field and the geometry of surfaces with which target cells interact must be considered and assessed.

The drag experienced by a bluff structure is composed of two parts: frictional drag and pressure drag. The skin friction along the fluidporous interface is much reduced compared with the solidfluid interface as the vorticity strength is lower in the former case. Besides, the pressure drop along the fluidporous interface is also lower compared with a solidfluid interface at a fixed Reynolds number. Thus, the total drag experienced by a porous-wrapped solid cylinder will be lower than a solid

cylinder of equal radius. The order of drag reduction must vary with the permeability of the porous material. By varying Da, we found that the increase in permeability of the porous layer produces reduction in drag coefficient.

Here we have varied the porous layer thickness up to four times the radius of the solid cylinder. Drag increases with the increase in surface area and reduces with the increase in Re. However, it is evident from Figure that C_d of a porous-wrapped cylinder is lower when compared with a solid cylinder of equal radius.

We have also varied the permeability of the porous medium, i.e. $Da = 10^2 to 10^5$. A significant drag reduction through the inclusion of porous wrapper is evident from this result. As the porous layer becomes more permeable, resistance experienced by the fluid in passing through the porous layer is less and thus the drag experienced by the porous-wrapped cylinder is lower.

The graph provides a guideline for optimal value of the porous layer thickness to construct a structure composed of inner solid body of radius a and a porous sheath of thickness $(b-a)$ so as to have a drag reduction of desired order. We find that increase in porous layer thickness produces a substantial drag reduction at a fixed value of the permeability. The drag on the composite structure can be reduced also by increasing the permeability. With the decrease in permeability the resistance to fluid flow in the porous zone increases; this gives rise to an increment in drag coefficient.

3.4 Effect of Velocity on Capture Efficiency

The inlet velocity plays an important role in the flow through the chip. The present chapter is directed towards the effects of varying the inlet velocity and studying its influence on the capture efficiency of the microfluidic chip. The impact of change in inlet velocity affects two primary parameters. Firstly, it determines the duration of contact of particles viz. rare cells with the cylindrical posts. Higher inlet velocity would lead to lesser duration of contact between the fluid and the posts. As this

contact time reduces, the susceptibility of the cells being captured reduces as will be demonstrated through simulations for varying inlet velocities.

Secondly, a high inlet velocity would increase the maximum velocity in the flow. This would in turn lead to an increase in shearing forces. As the shearing forces increases, a particle that would normally be captured on the surface of the cylindrical post would be sheared off and displaced. There is a high chance that this displaced particle may not come in contact with the subsequent columns of cylindrical micro posts thereby reducing the overall capture efficiency of the chip. Also a high shear force is undesirable as it reduces the maximum cell-micropost attachment.

For the purpose of the study, the range of Reynolds number lies from $0.01 \leq Re \leq 0.15$ for a range of velocity lying between $100 \leq V_{in} \leq 1500\ \mu m/s$. For creeping flow condition of $Re \ll 1$, the chosen range of Reynolds number is in total fulfillment of this condition. This can be supported by the initial test simulations where the applicability of the full Navier-Stokes equation and simplified Stokes equation were tested. For $Re = 0.15$, the overall capture efficiency were the same for both the aforementioned cases. Hence $Re = 0.15$ satisfies the creeping flow condition.

Inlet velocity = $100\ \mu m/s$

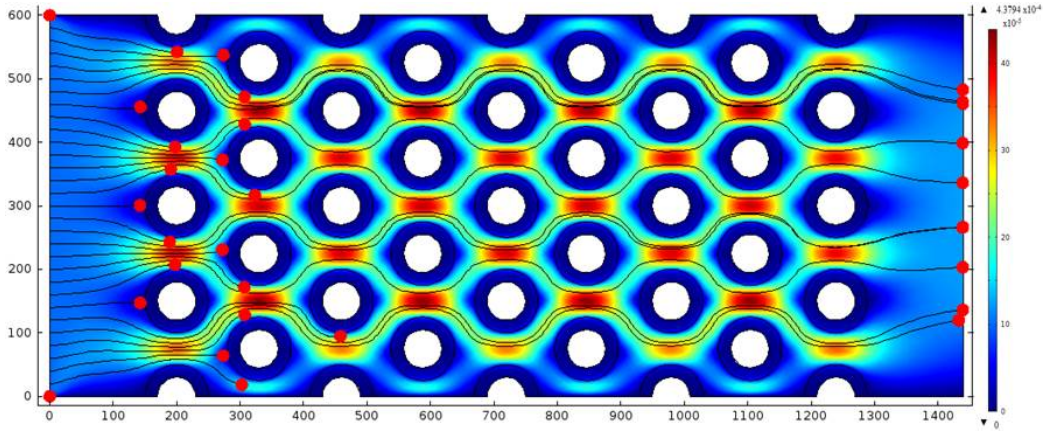

Figure 3.16. Variation of inlet velocity. The simulation result is for an initial release of 30 particles.

Inlet velocity = 300 $\mu m/s$

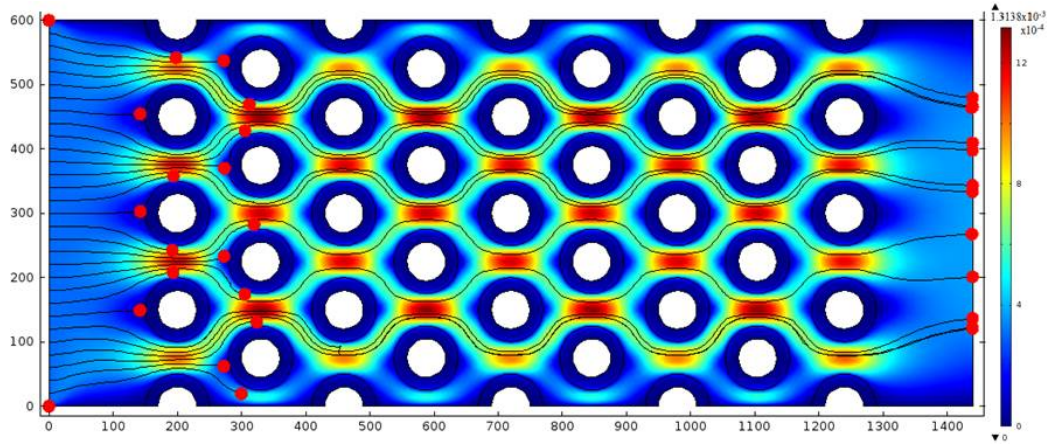

Figure 3.17. Variation of capture efficiency with an inlet velocity = 300 $\mu m/s$.

Inlet velocity = 500 $\mu m/s$

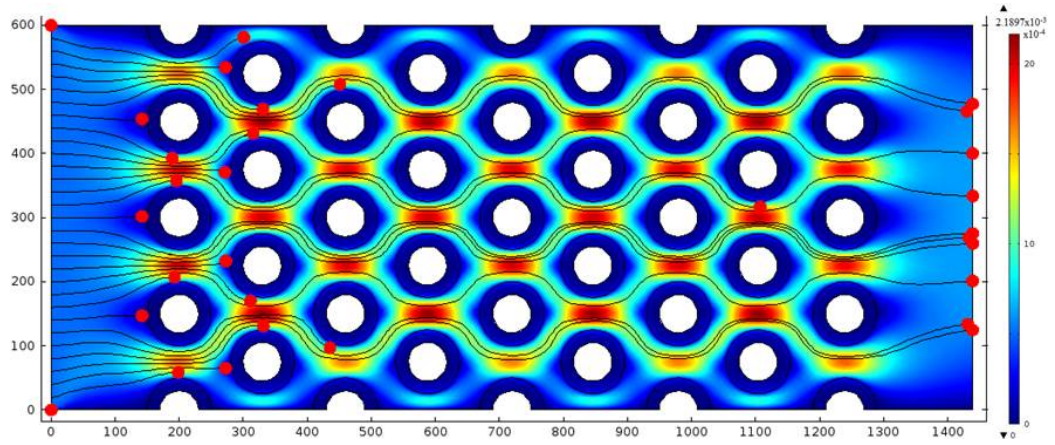

Figure 3.18. Variation of capture efficiency with an inlet velocity = 500 $\mu m/s$.

Inlet velocity = 700 $\mu m/s$

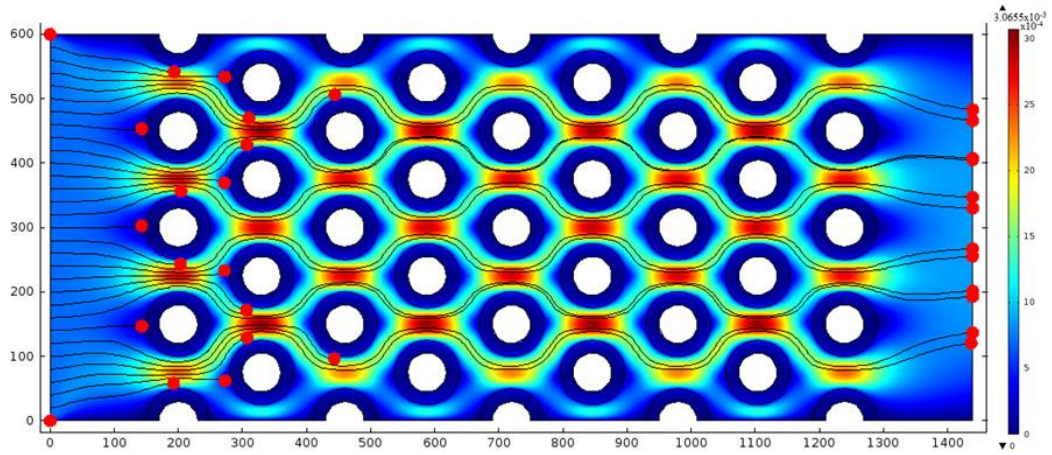

Figure 3.19. Variation of capture efficiency with an inlet velocity = 700 $\mu m/s$.

Inlet velocity = 900 $\mu m/s$

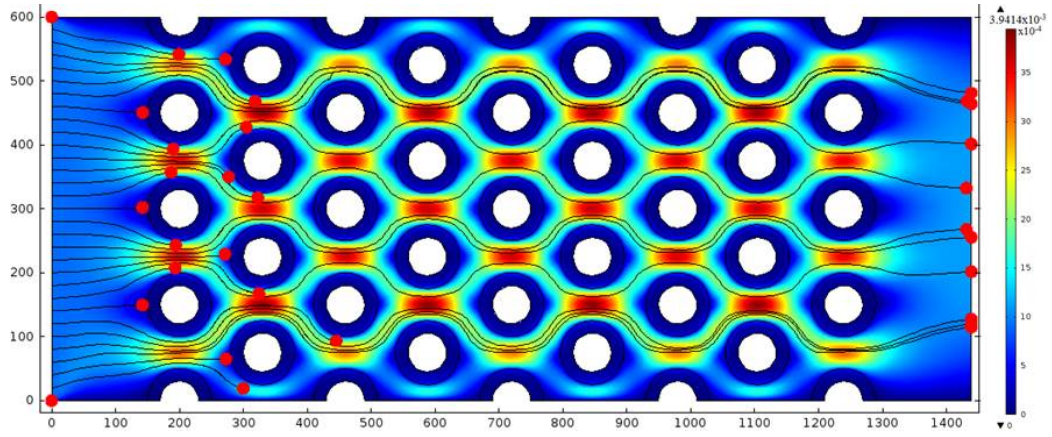

Figure 3.20. Variation of capture efficiency with an inlet velocity = 900 $\mu m/s$.

Inlet velocity = 1200 $\mu m/s$

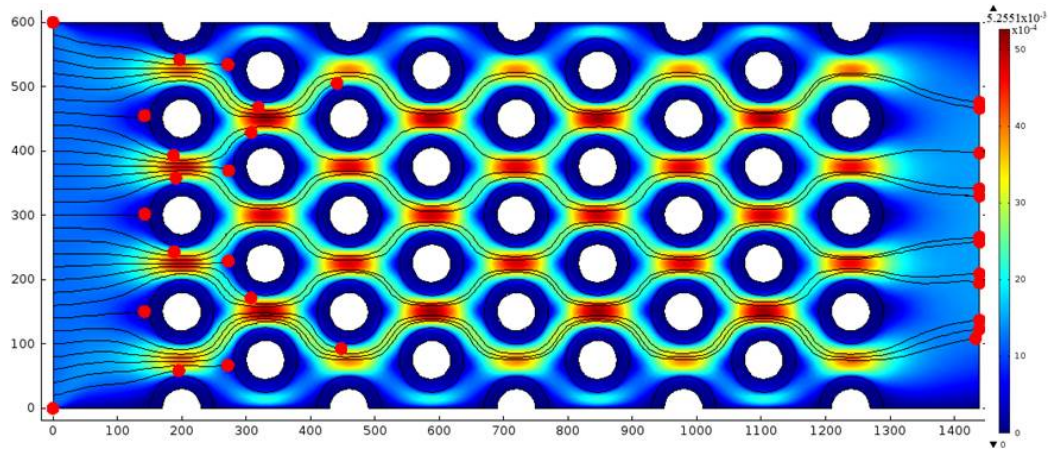

Figure 3.21. Variation of capture efficiency with an inlet velocity = 1200 $\mu m/s$.

Inlet velocity = 1500 $\mu m/s$

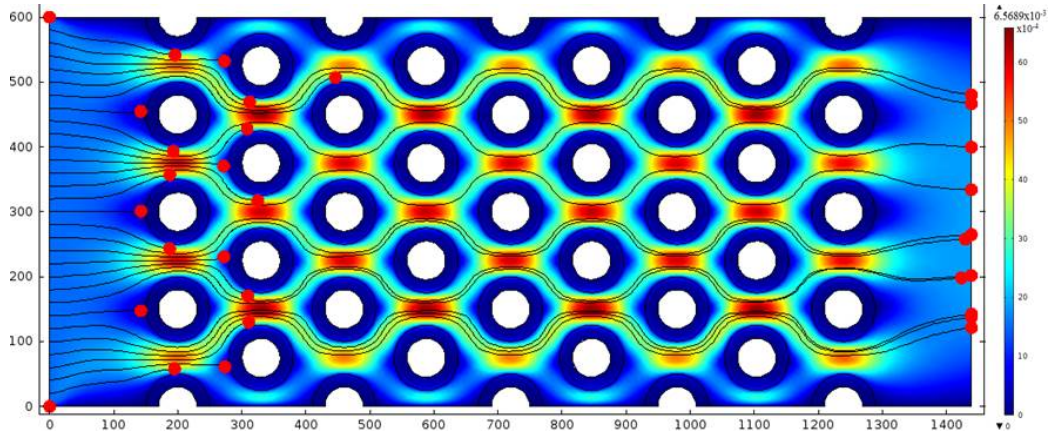

Figure 3.22. Variation of capture efficiency with an inlet velocity = 1500 $\mu m/s$.

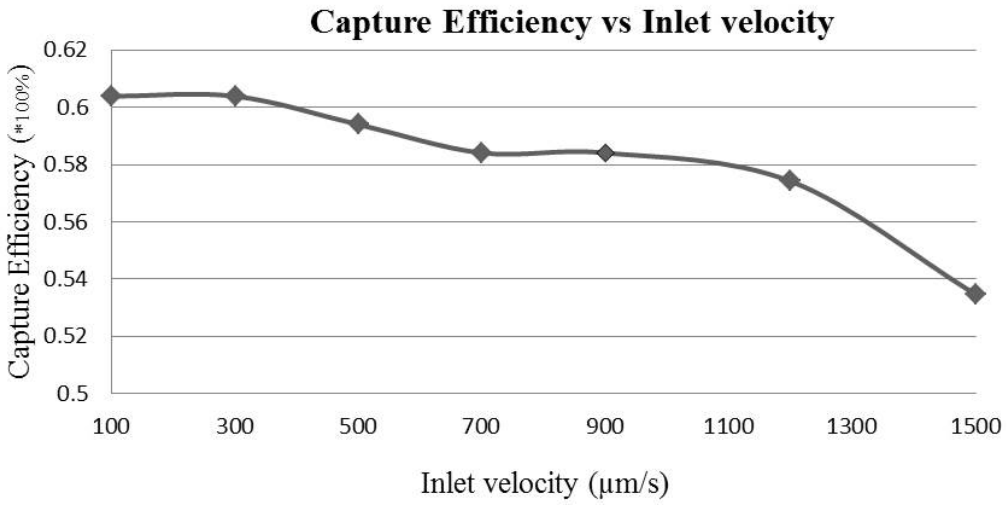

Figure 3.23. The variation of capture efficiency with the inlet velocity. With the increase in inlet velocity the capture efficiency is gradually decreased.

The following simulation results are for completely solid posts under similar conditions as that of the composite posts. The two designs will be compared and it will be shown how the composite posts have higher capture efficiency.

Inlet velocity = 100 $\mu m/s$

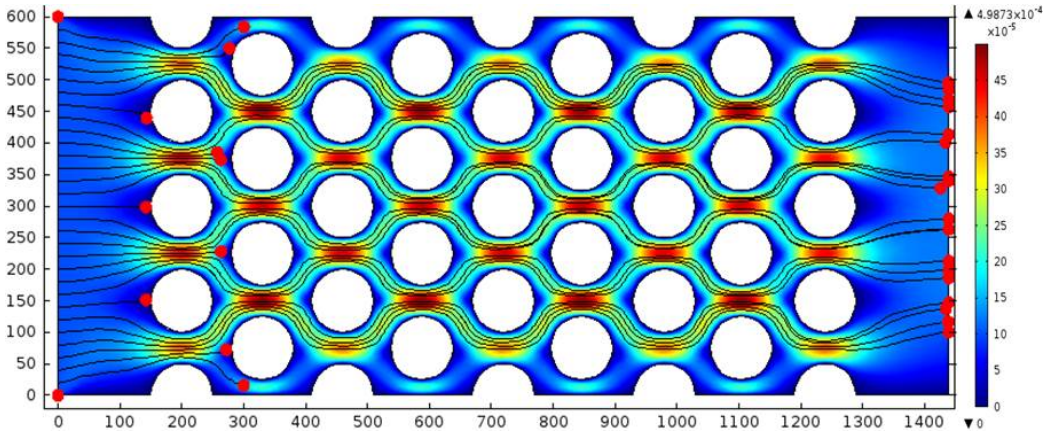

Figure 3.24. Variation of capture efficiency with an inlet velocity = 100 $\mu m/s$.

Inlet velocity = 300 $\mu m/s$

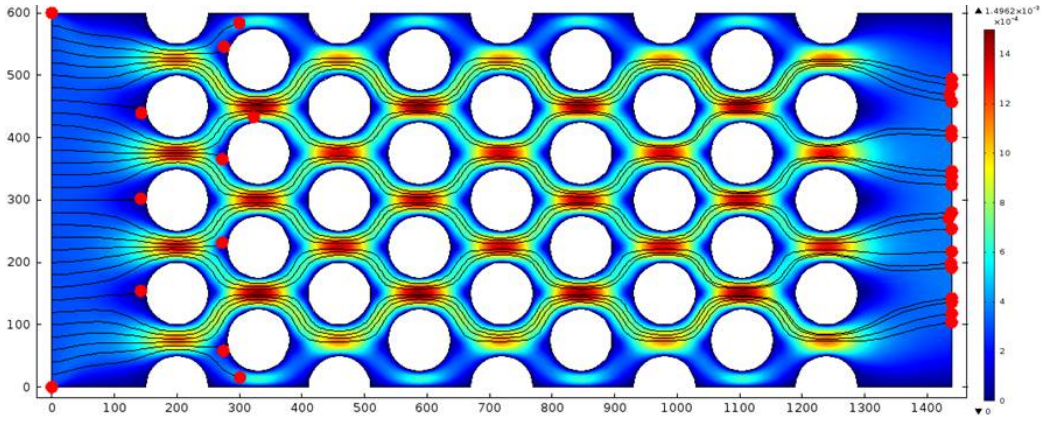

Figure 3.25. Variation of capture efficiency with an inlet velocity = 300 $\mu m/s$.

Inlet velocity = 500 $\mu m/s$

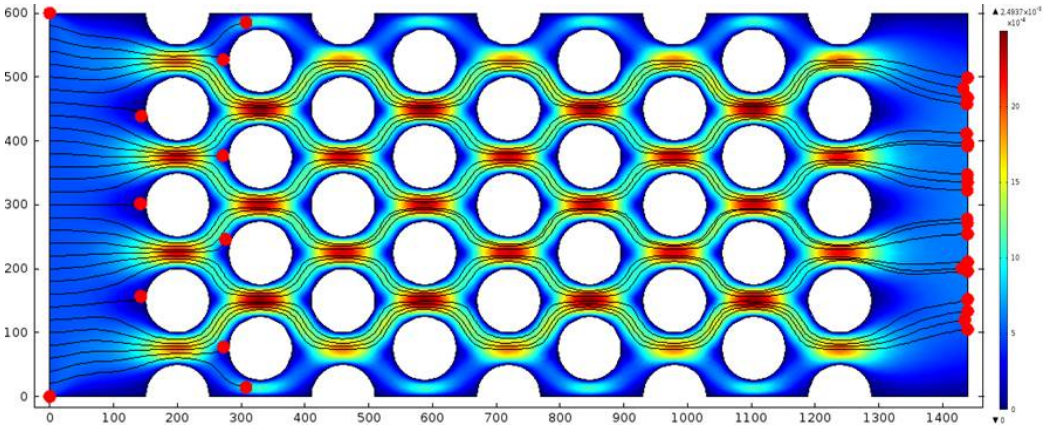

Figure 3.26. Variation of capture efficiency with an inlet velocity = 500 $\mu m/s$.

Inlet velocity = 700 $\mu m/s$

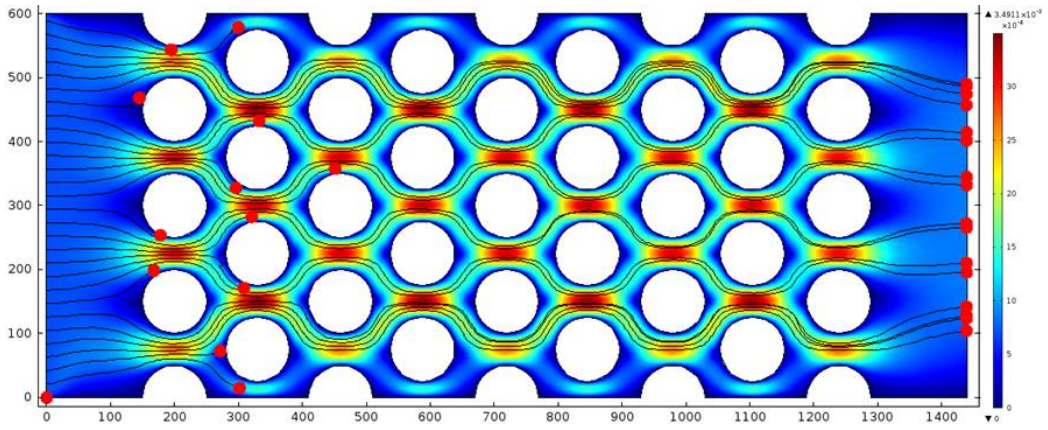

Figure 3.27. Variation of capture efficiency with an inlet velocity = 700 $\mu m/s$.

Inlet velocity = 900 $\mu m/s$

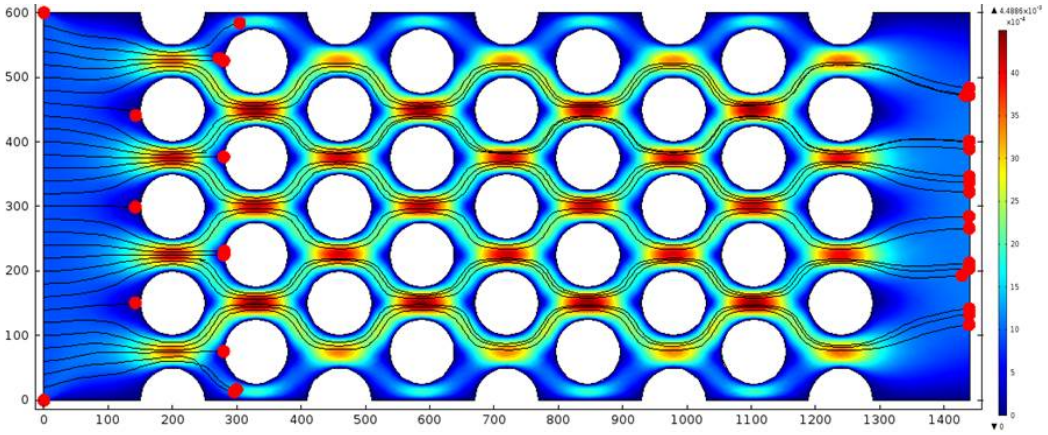

Figure 3.28. Variation of capture efficiency with an inlet velocity = 900 $\mu m/s$.

Inlet velocity = 1200 $\mu m/s$

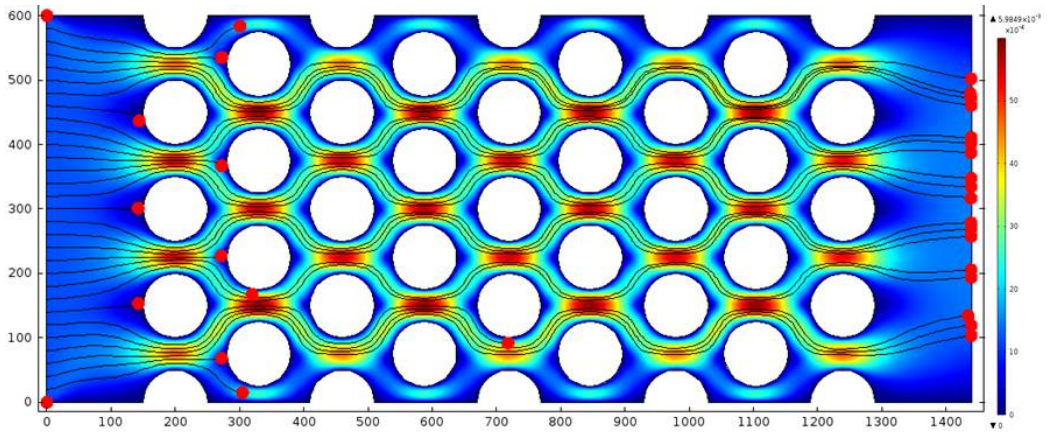

Figure 3.29. Variation of capture efficiency with an inlet velocity = 1200 $\mu m/s$.

Inlet velocity = 1500 $\mu m/s$

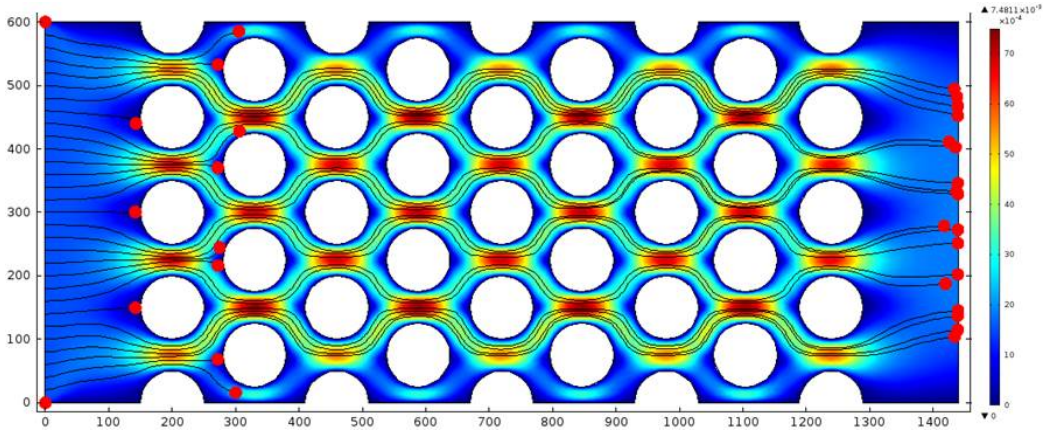

Figure 3.30. Variation of capture efficiency with an inlet velocity = 1500 $\mu m/s$.

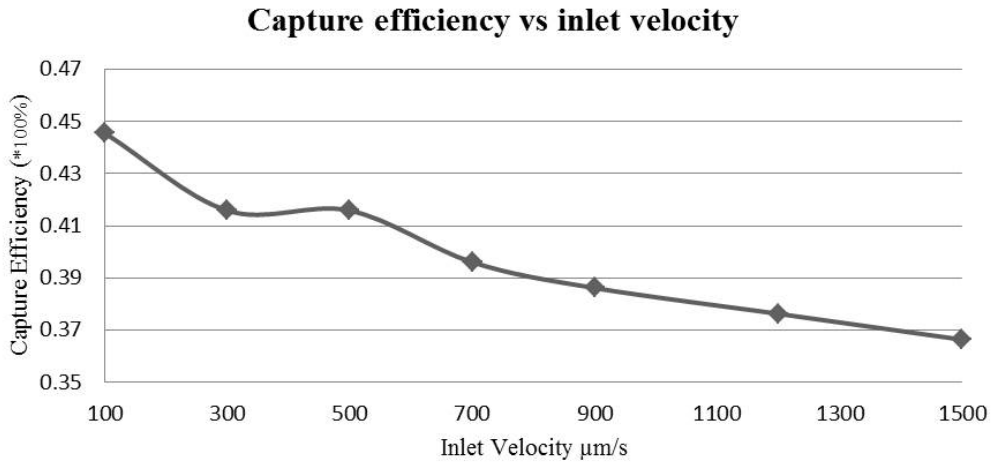

Figure 3.31. The variation of capture efficiency with the inlet velocity. As similar to the composite posts, with the increase in inlet velocity the capture efficiency is gradually decreased.

The initial velocity was varied for the initial chip design that was chosen. As expected, as the velocity increases due to the reduction in cell-micropost attachment and duration of cell-micropost contact, the capture efficiency gradually decreases. These results are compared to a chip design consisting of completely solid microposts. It is seen that for a similar arrangement of solid microposts, the capture efficiency is greatly declining with the increase in velocity as the shearing forces increases. Due to the presence of the porous sheath covering in the initial chip design of solid core cylinder and porous shell, the shearing forces are reduced and the duration of contact between the post and cells is higher. Therefore, this introduced technique of solid core cylinder with porous shell covering is a more efficient way of capturing rare cells compared to the previously used models of incorporating only solid microposts.

3.5 Effect of Arrangement of Posts on Capture Efficiency

Deformable cells or particles traveling along surfaces experience a force away from the surface; this force works against rare cell-capture devices. Although this force

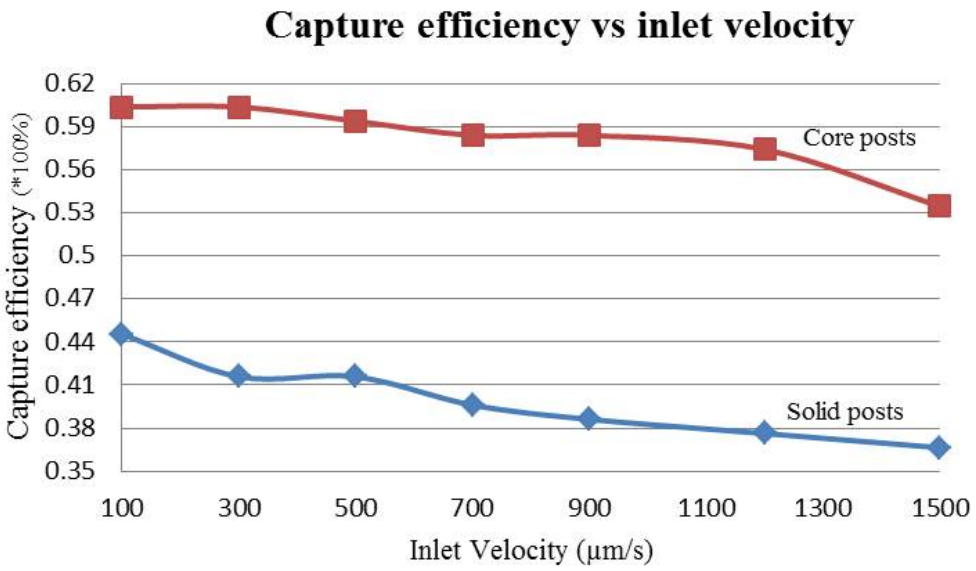

Figure 3.32. The comparison in capture efficiency of the design that utilizes a solid post with a porous sheath and the design that uses only solid posts. It can be observed that the first design, i.e. the composite posts design has a higher capture efficiency than that of only the solid posts under similar conditions.

is important in many applications, rare cell-capture micro-devices are typically designed to specifically avoid or overwhelm this force, and a detailed description of this effect rarely plays a central role in describing device performance. In contrast, the displacement associated with cell-wall collisions and the downstream effect of these collisions is often a central factor.

As a particle travels along a streamline that approaches a solid boundary, the finite size of the particle prevents its center from moving closer than one particle radius (for a rigid spherical particle) to the boundary; more generally, deformable and non-spherical particles in general have a geometry and rigidity-specific approach distance. Regardless of the details, the result is that the center of rare cells has a minimum distance from the surface; if the streamline on which a cell is traveling approaches the surface more closely than this distance, the resulting collision displaces the cell from the initial streamline and the cell pathline deviates from that streamline.

The initial arrangement of posts consisted of an equilateral triangle arrangement. In this type of arrangement has yielded decent results both in the present study as well as in previous literature pertaining to this field. The focus of the present chapter will be to modify this initial arrangement of posts such that the capture efficiency of the rare cells is enhanced. To begin, we start with the assumption that the particle has a radius which is about 9 μm. If the particles are not captured by the first column of microposts, one may think that the minimum distance by which the next column of posts might be displaced is by a distance at least equal to that of the particle radius. The outcome of this new geometry is to maximize the streamline distortion such that the desired rare cells are brought in contact with the microposts. Since blood is a dense viscous liquid consisting of cells of various sizes, the rare cells are usually larger than that of the normal blood cells and this feature of the rare cells is utilized to improve the capture efficiency. The relative microposts alignment was chosen so that the displacement caused by the cell impact with the posts increases the likelihood of future cell impacts for larger cells. Thus when the cell-post impact does not lead to capture, the larger cells are displaced onto streamlines that impinge on the next column of posts.

The new improvement in the design was to shift the column of cylindrical posts. Every $4n^{th}$ row will have an upward shift and every $4n+2^{th}$ row will have a downward shift. n refers to the column number. The columns are shifted to bring about a change in the path of the particles and this may increase the collision efficiency between the particles and the posts thereby increasing the overall capture efficiency. Fig. 3.33 depicts the new arrangement and shows the shift the in the columns of posts.

The minimum distance by which the columns of posts are shifted is 9 μm considering that it is the cell radius. To find the optimum displacement that leads to higher capture efficiency, the shifts in the columns was increased from 9 μm to 15 μm.

A shift in the horizontal displacement of the columns was not considered as that would just obstruct the flow and would not serve the purpose of distorting the streamlines which is the main aim of this arrangement. Once the optimum shift is found

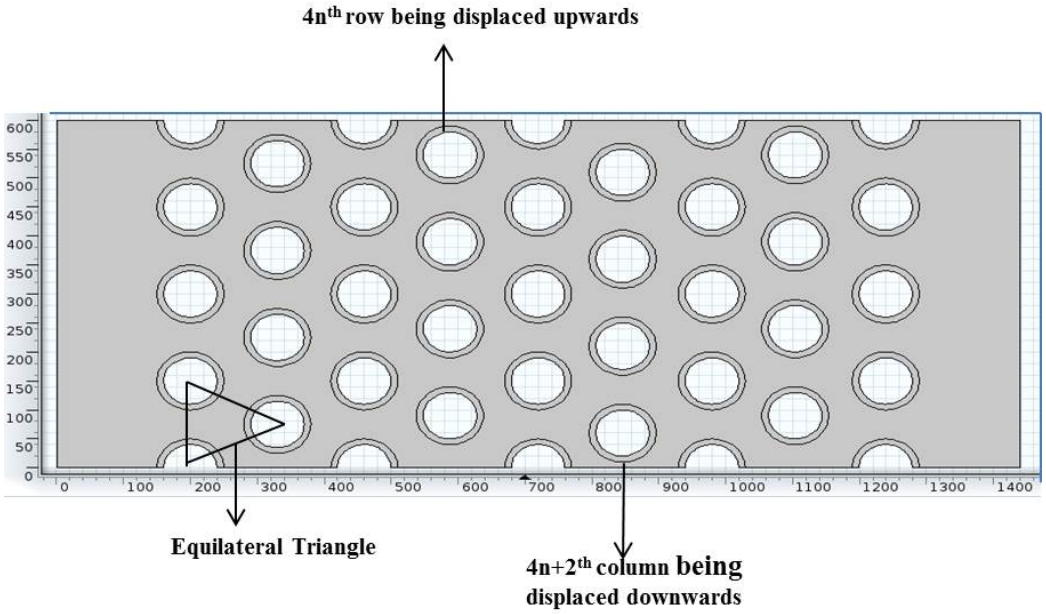

Figure 3.33. The change from the initial design. The first two rows are in an equilateral arrangement from the initial design. The incorporation of the shifts in the $4n^{th}$ and $4n+2^{th}$ row is shown. The shift is shown for 15 μm.

the design is applied for completely solid cylindrical posts. It will be noticed that even though solid cylindrical posts are used, due to the column shifting there is an increasing in the capture efficiency when compared to the design without the shift in the microposts. With the help of simulations, the capture efficiency of the new design will be compared to that of the initial design for both solid cylindrical posts as well as for solid cylinder with porous shell covered posts. It is interesting to note that a mere shift in the posts can lead to increased capture efficiencies.

Displacement = 20 μm

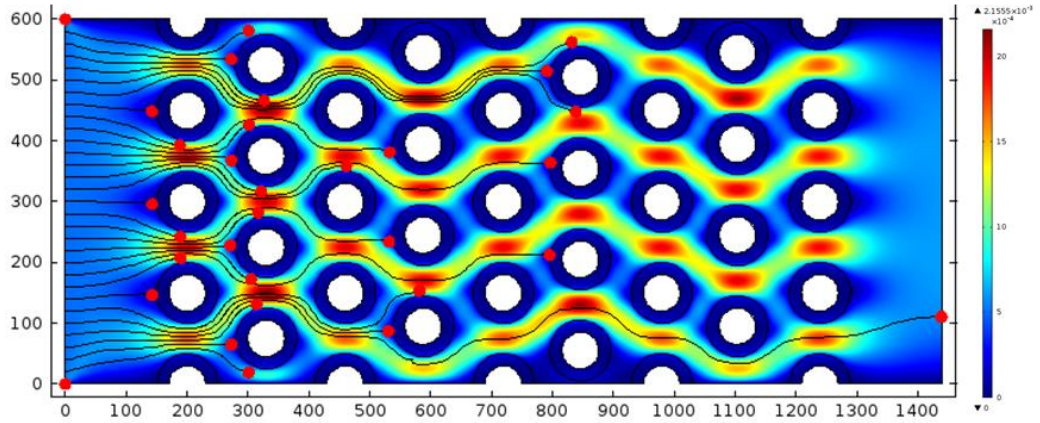

Figure 3.34. The number of particles being captured for a shift of 20 μm.

Displacement = 15 μm

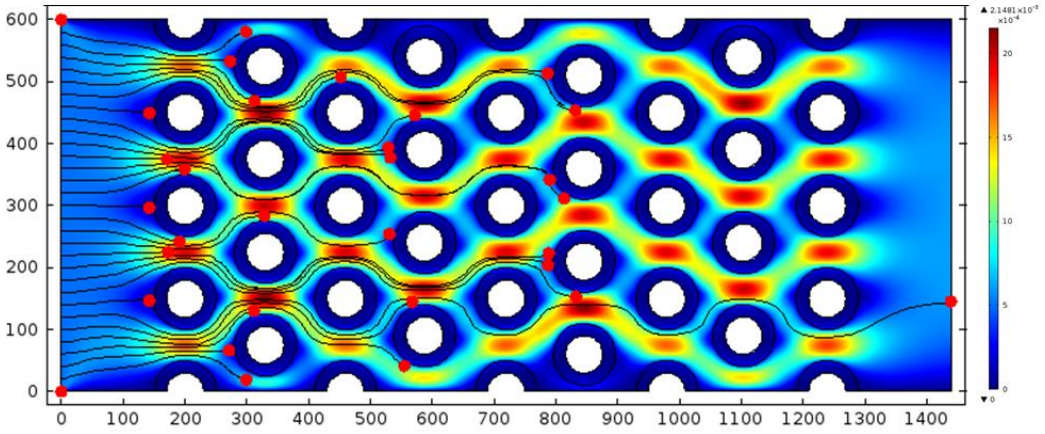

Figure 3.35. The number of particles being captured for a shift of 15 μm.

Displacement = 12 μm

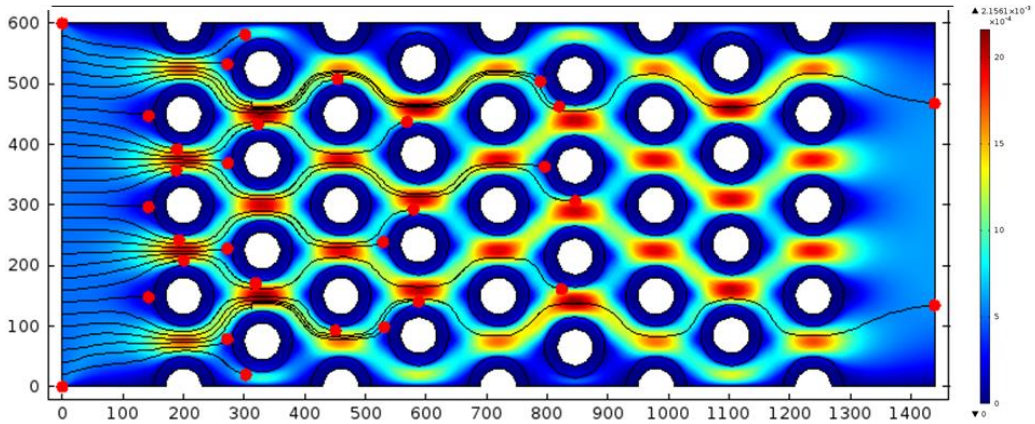

Figure 3.36. The number of particles being captured for a shift of 12 μm.

Displacement = 10 μm

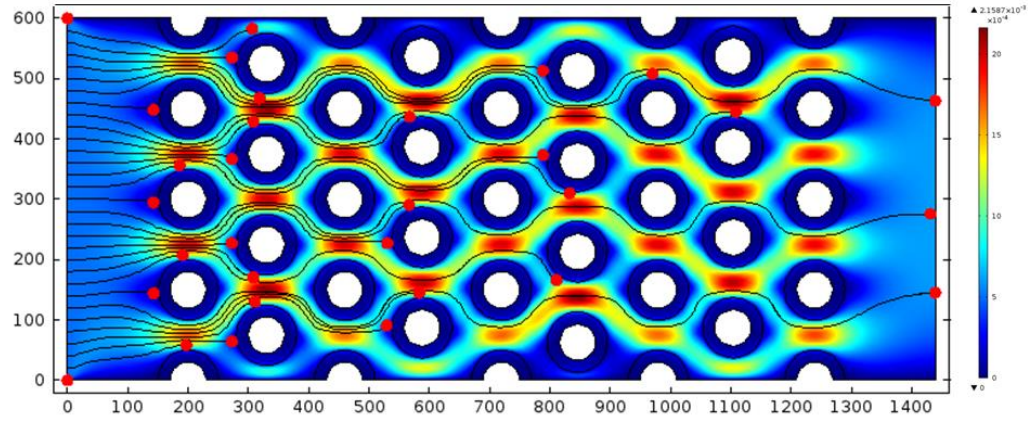

Figure 3.37. The number of particles being captured for a shift of 10 μm.

Displacement = 9 μm

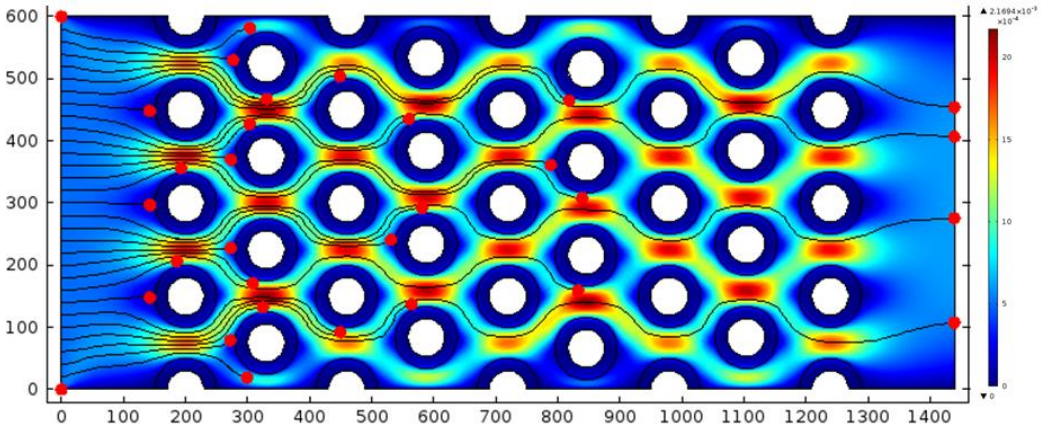

Figure 3.38. The number of particles being captured for a shift of 9 μm.

Displacement = 8 μm

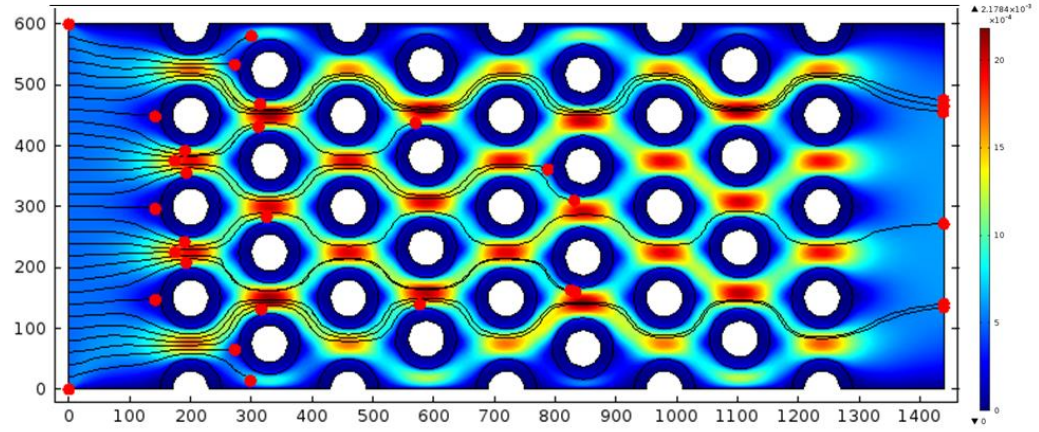

Figure 3.39. The number of particles being captured for a shift of 8 μm.

Displacement = 5 μm

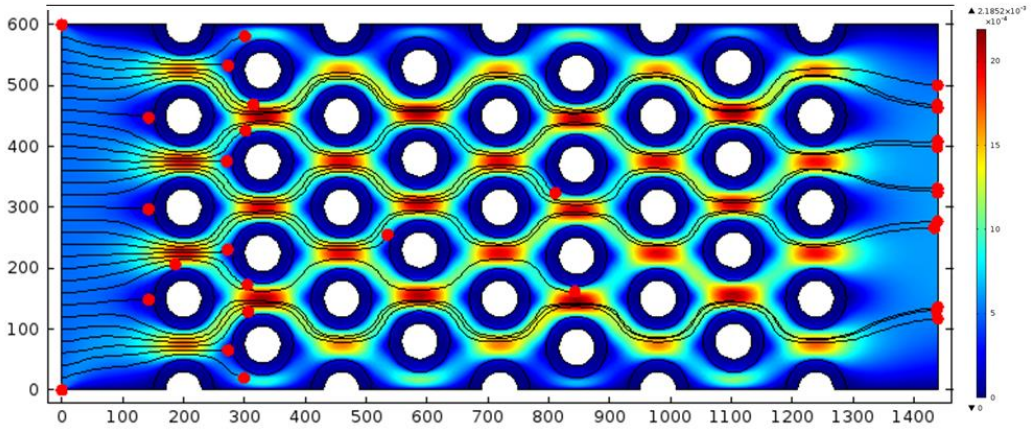

Figure 3.40. The number of particles being captured for a shift of 5 μm.

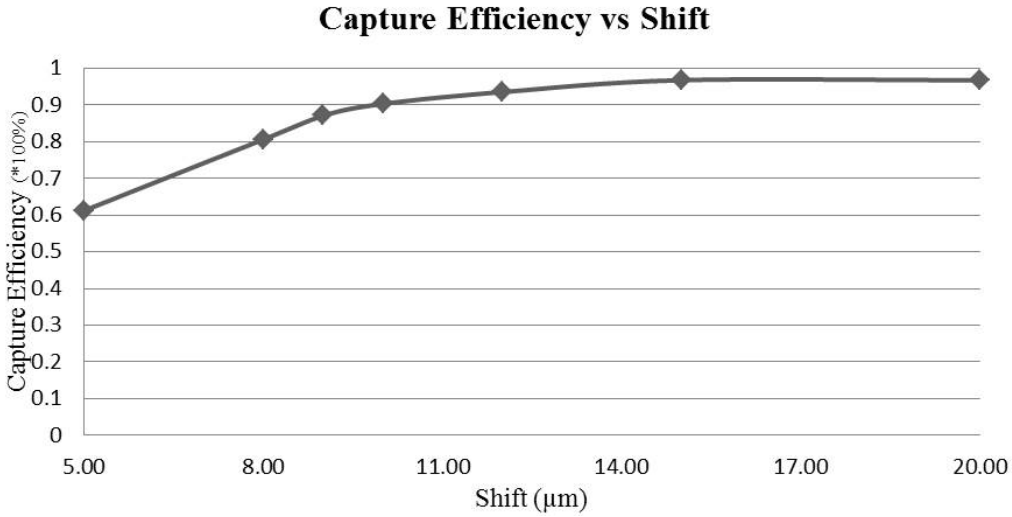

Figure 3.41. The behavior of capture efficiency with the increase in shift in the columns of microposts.

It is noted that as the shift increases the capture efficiency increases. We started the shift with 5 μm and went on to 20 μm. As we had an initial assumption that the column shift must be at least 9 μm, we found the capture efficiency at that value of shift. It rendered an efficiency of 87%. As we increased the shift to 15 μm, the

capture efficiency jumped to 96.77%. Though the capture efficiency for 15 μm and 20 μm shift are the same, an optimized shift of 15 μm is accepted as the maximum velocity in the flow is lesser than that of the 20 μm shift. This design is the new optimized model of the microfluidic chip for rare cell isolation.

3.6 Optimized Design for Higher Yield

The goal of optimizing a microfluidic chip for rare cell isolation is to improve the capture efficiency. Another important factor is the yield of the device. A desirable yield is achieved when the duration for the completion of the process is not high. One way to achieve higher yield is to increase the inlet velocity. As the inlet velocity is increased, since the flow becomes faster, the process is completed in a lesser duration of time. But as the inlet velocity increases, the cell-post attachment is reduced and a decrease in the capture efficiency can be expected. However, we will show with the support of simulations how the new optimized design has relatively higher capture efficiency even with the increase in inlet velocity. The maximum velocity in the flow is obviously increased but is comparatively lower than the initial design used. For lower inlet velocities the capture efficiency is the highest but the yield is low and the frequency of usability of the chip is reduced. With the help of simulations, the change in inlet velocity and its effect on capture efficiency will be shown.

Inlet Velocity = 300 $\mu m/s$

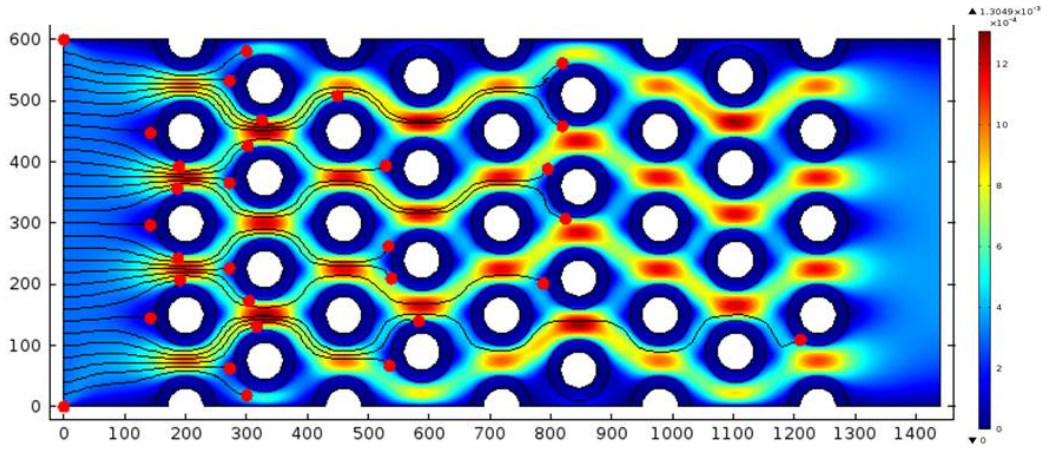

Figure 3.42. The cells being captured for an inlet velocity = 300 $\mu m/s$ for the optimized design.

Inlet Velocity = 500 $\mu m/s$

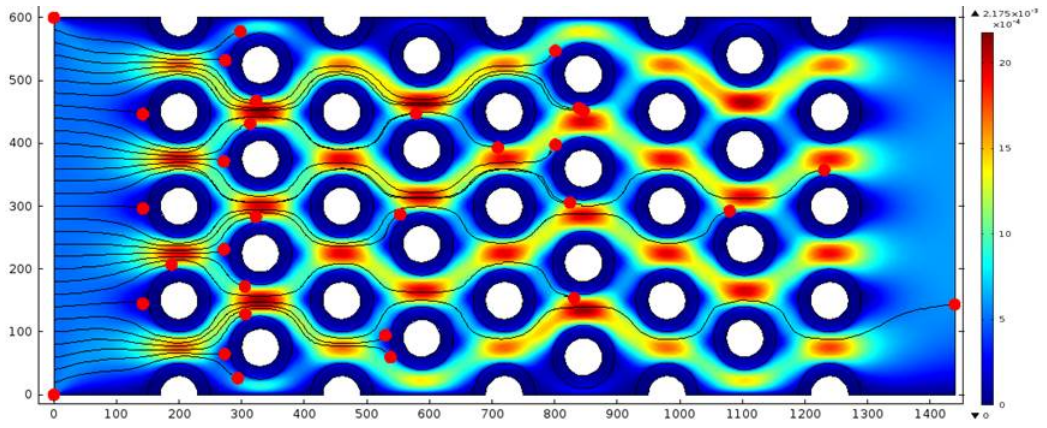

Figure 3.43. The cells being captured for an inlet velocity = 500 $\mu m/s$ for the optimized design.

Inlet Velocity = 700 $\mu m/s$

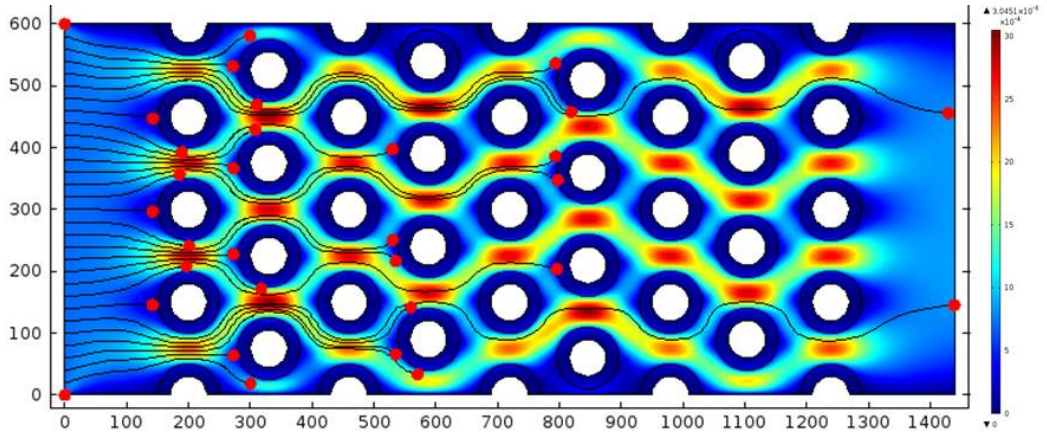

Figure 3.44. The cells being captured for an inlet velocity = 700 $\mu m/s$ for the optimized design.

Inlet Velocity = 900 $\mu m/s$

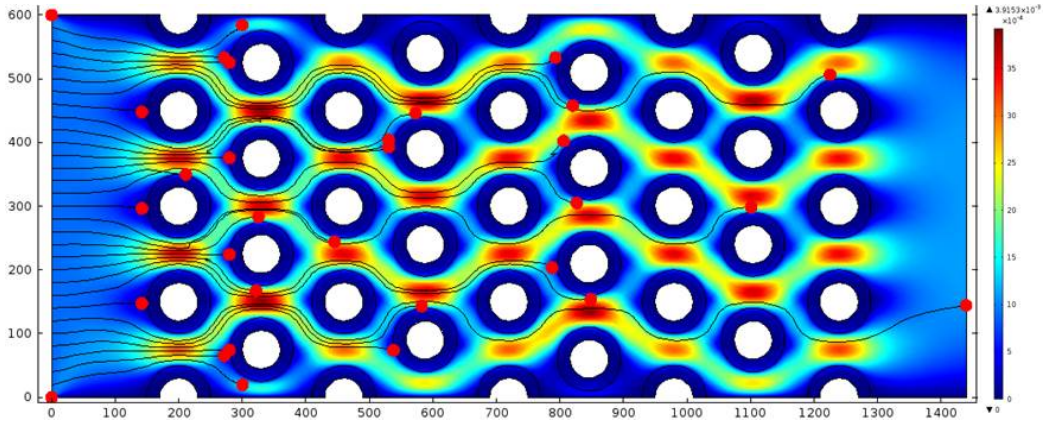

Figure 3.45. The cells being captured for an inlet velocity = 900 $\mu m/s$ for the optimized design.

Inlet Velocity = 1200 $\mu m/s$

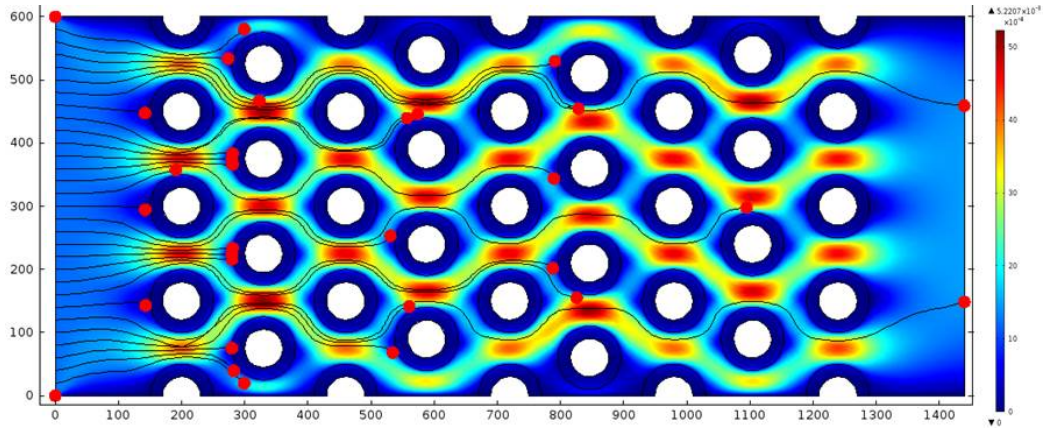

Figure 3.46. The cells being captured for an inlet velocity = 1200 $\mu m/s$ for the optimized design.

Inlet Velocity = 1500 $\mu m/s$

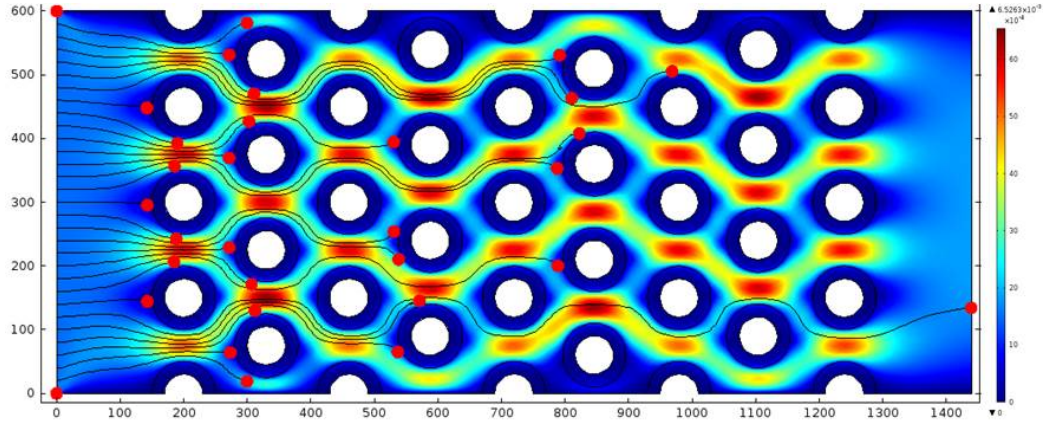

Figure 3.47. The cells being captured for an inlet velocity = 1500 $\mu m/s$ for the optimized design.

Inlet Velocity = 2000 $\mu m/s$

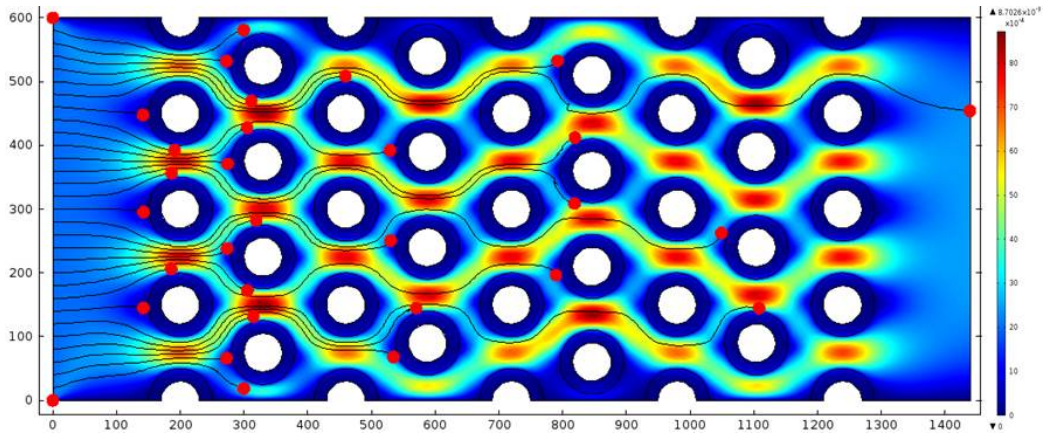

Figure 3.48. The cells being captured for an inlet velocity = 2000 $\mu m/s$ for the optimized design.

The simulations show the change in inlet velocity as compared to the capture efficiency. They show for an approximate of thirty particles that are allowed into the flow. However, the capture efficiency that will be shown in the graph will be for about hundred particles that are allowed to enter the flow.

Fig. 3.49 shows how the capture efficiency decreases with the increase in inlet velocity. As expected, the capture efficiency is gradually decreasing with the increase in velocity. But it can also be noticed that though the inlet velocity is as high as 2000 μm the capture efficiency is approximately 94% which is quite a commendable efficiency. Such high efficiencies are achieved due to the arrangement of the posts and the porous sheath covering around the solid core cylinder. The maximum velocity in the flow is very high and there is a high chance that the particles that are captured also may shear off from the posts. But due to the arrangement of posts to increase the collision efficiency the particles that are sheared off come in contact with the succeeding columns of microposts thereby still retaining high capture efficiencies.

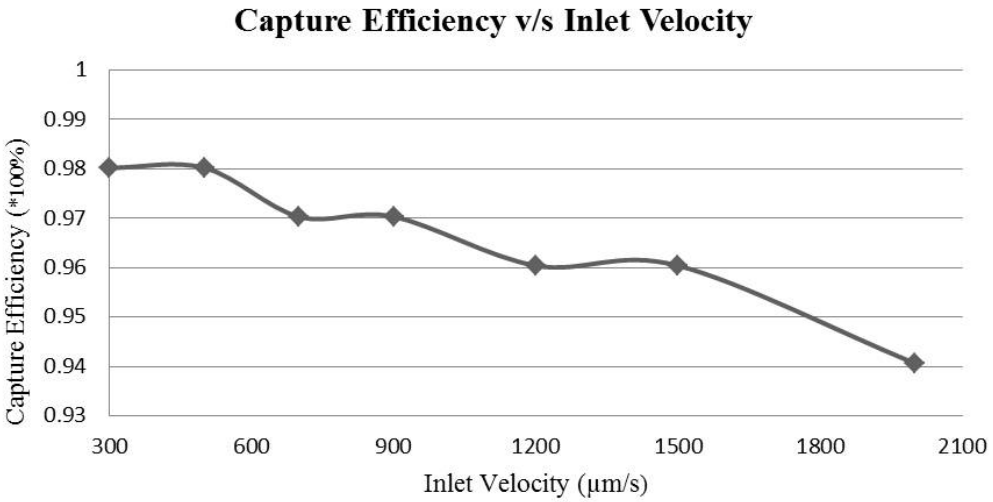

Figure 3.49. The behavior of capture efficiency for increasing velocity. Even for a high inlet velocity, the capture efficiency is a little more than 94% which testifies the optimized design. Also this proves that the throughput of the chip is high.

If the same optimized design is applied to the chip with completely solid posts, the efficiency is greatly increased. Below is the comparison of the solid posts design before being optimized and after being optimized.

Inlet Velocity = 300 $\mu m/s$

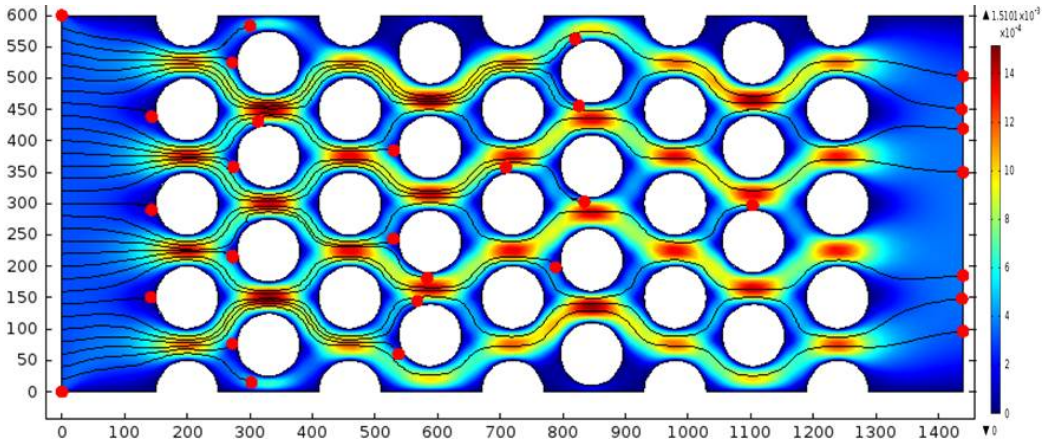

Figure 3.50. The optimized design being applied to the solid posts with an inlet velocity = 300 $\mu m/s$.

Inlet Velocity = 500 $\mu m/s$

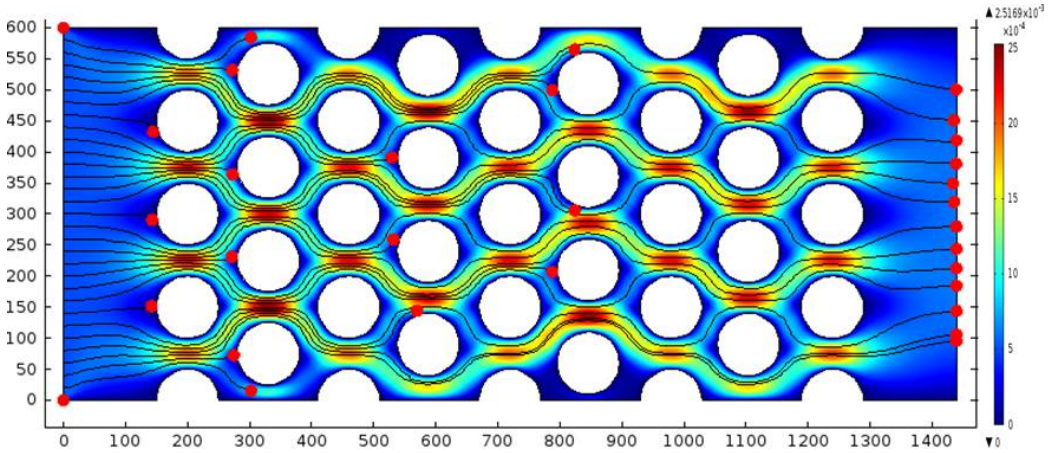

Figure 3.51. The optimized design being applied to the solid posts with an inlet velocity = 500 $\mu m/s$.

Inlet Velocity = 700 $\mu m/s$

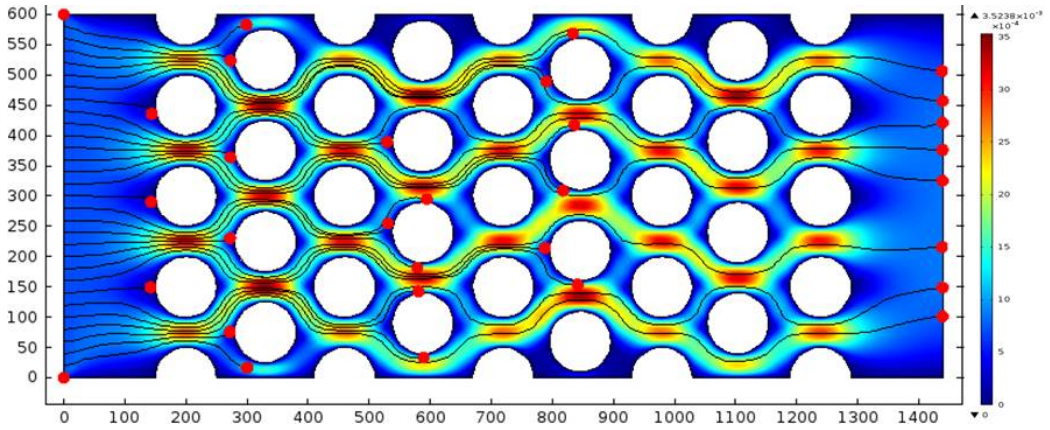

Figure 3.52. The optimized design being applied to the solid posts with an inlet velocity = 700 $\mu m/s$.

Inlet Velocity = 900 μm/s

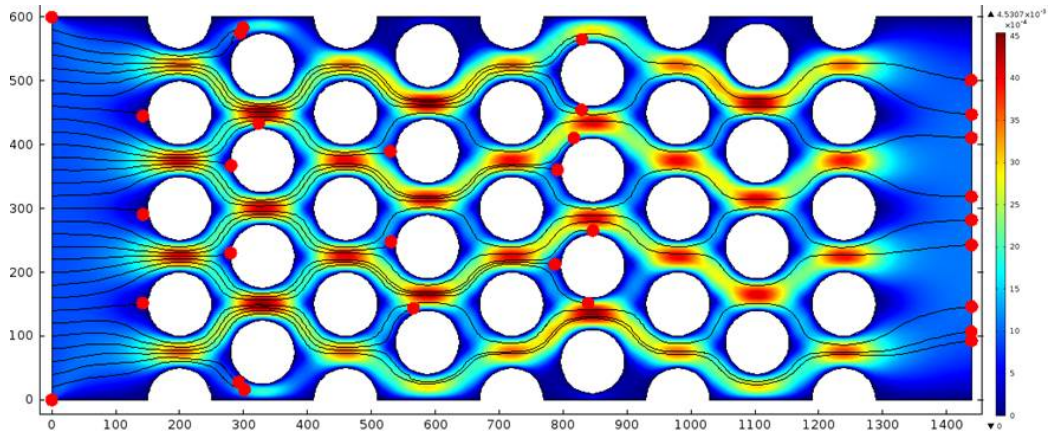

Figure 3.53. The optimized design being applied to the solid posts with an inlet velocity = 900 $\mu m/s$.

Inlet Velocity = 1200 $\mu m/s$

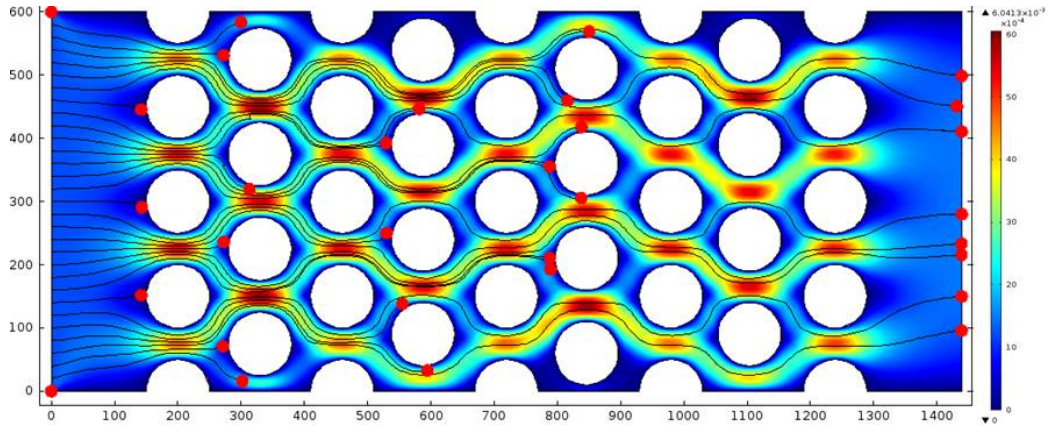

Figure 3.54. The optimized design being applied to the solid posts with an inlet velocity = 1200 $\mu m/s$.

Inlet Velocity = 1500 $\mu m/s$

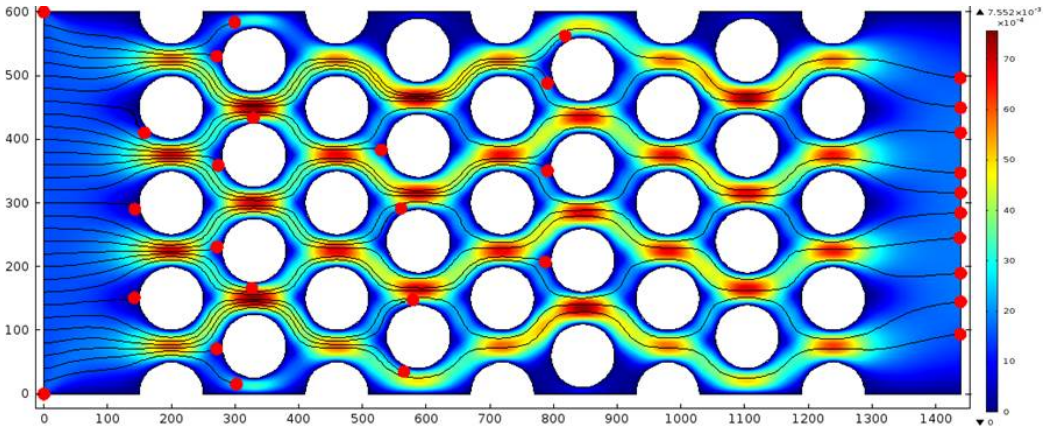

Figure 3.55. The optimized design being applied to the solid posts with an inlet velocity = 1500 $\mu m/s$.

Inlet Velocity = 2000 $\mu m/s$

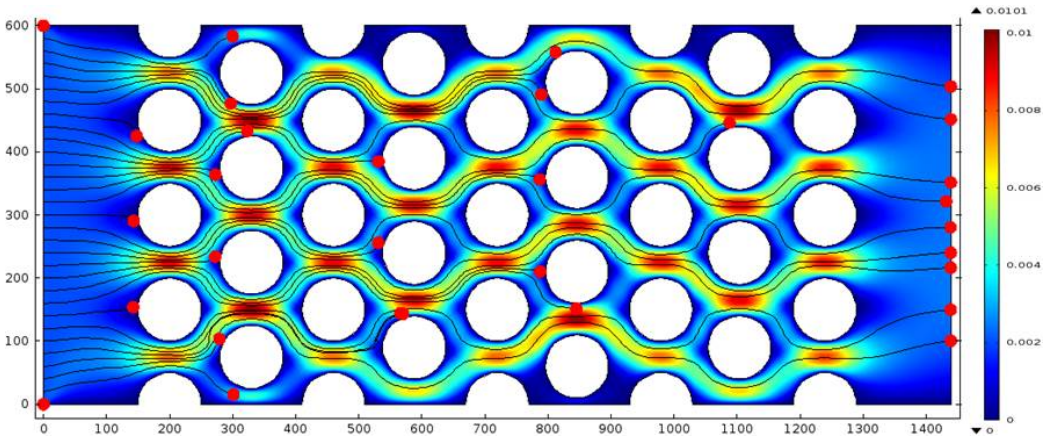

Figure 3.56. The optimized design being applied to the solid posts with an inlet velocity = 2000 $\mu m/s$.

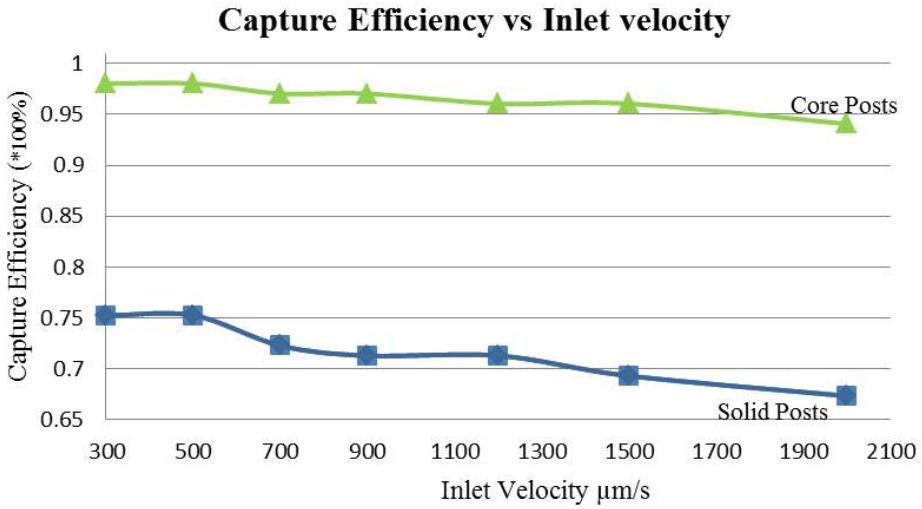

Figure 3.57. The comparison between the capture efficiency for a composite post design and a solid posts design. The composite posts have a higher capture efficiency and therefore prove to be a better design.

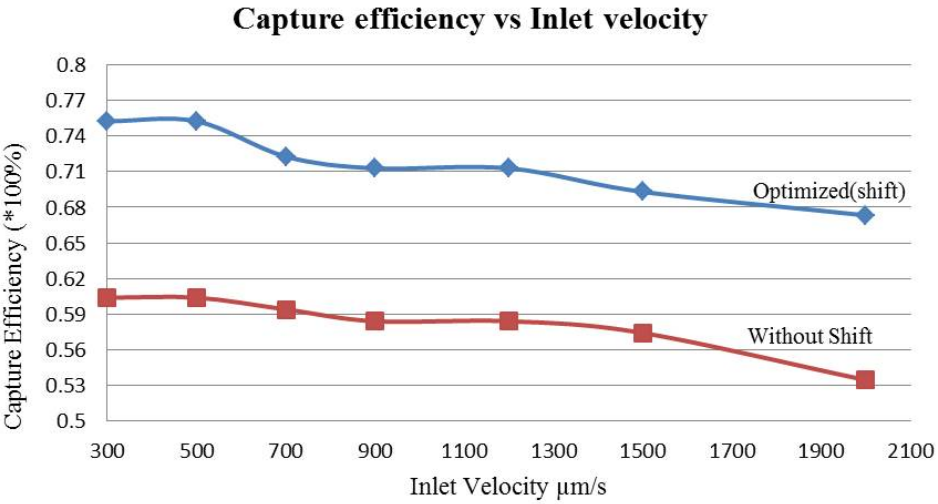

Figure 3.58. The comparison in capture efficiency for the design utilizing only completely solid microposts before being optimized and after being optimized.

The optimization process is thus finalized by proving how the capture efficiency of a design that uses composite microposts is higher than that of the design that uses only completely solid microposts. It is also shown that the optimized design stands good for a chip design that uses solid microposts by illustrating how the capture efficiency increases from 60% to 76% for the deduced optimized design.

4. FABRICATION PROCESS

In this research, we present the use of novel multiscale 3-dimensional structures coated with nucleic acid aptamers generated by in vitro cell-SELEX in a microfluidic platform for rare cell isolation applications, which can help to solve the challenges of low throughput, low capture efficiency, high hydrodynamic resistance and the high shear stress [15].

As shown in Fig. 4.1 a micro post array with core/shell structures is fabricated in a microchannel. The microstructure includes a solid core and a porous shell decorated with a silicon nanopillar (SiNP) forest. The microfluidic system with posts generates optimal flow characteristics and can increase the contact frequency and duration of interaction between rare cells and capturing elements. Nano-structures allow for enhanced local topographic interactions with nanoscale components of the cellular surface that are of comparable length scale as nanopillars. The interactions could result in improved cell-capture affinity when compared to unstructured (i.e., flat silicon surface) substrates and the smooth red blood cell surface. Compared to the flat surface, the nanopillar forest on the surface of micro posts would allow for reduced hydrodynamic resistance. Nucleic acid aptamers are conjugated to the surfaces of micro posts for improved cell capture. These aptamers have numerous merits for biological and biomedical applications, by virtue of their high binding affinity, specificity and robustness. Furthermore, their small size, tunable binding kinetics, ease of synthesis and little immunogenicity or toxicity are advantageous for providing capture functionality.

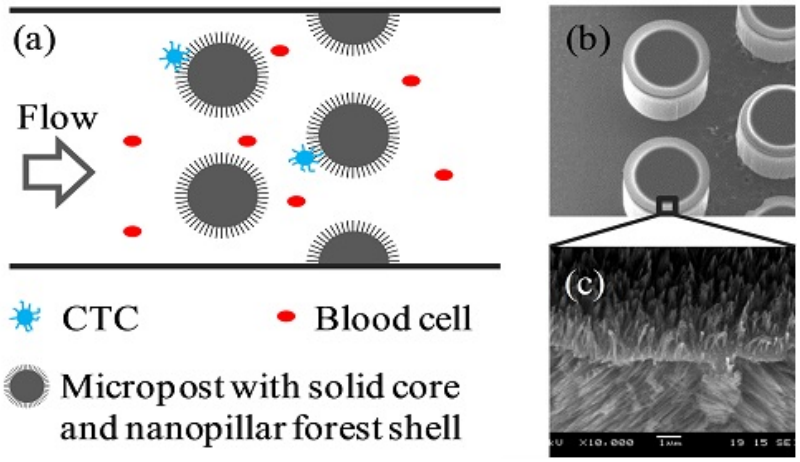

Figure 4.1. (a) Schematic of CTC isolation in a microchannel with micro post arrays. The micro post includes a solid core and a nanopillar forest shell. (b) A SEM image showing the micro post array with core/shell structure in a microchannel. (c) A SEM image showing the nanopillars on the surface of a micro post [15].

The microchannel and the micro posts were defined on a <100> silicon wafer with 1 μm thick low stress silicon nitride using a two-step deep reactive ion etching (DRIE) process. Aluminum was used as an additional DRIE protective mask. The fabrication process is depicted sequentially as follows.

Step 1: Isotropic SF_6 plasma was used to transfer pattern to the silicon nitride, with minimal undercut into the underlying silicon substrate and is shown in Fig. 4.2(A).

Step 2: The Bosch process was used to create the micro posts. The Bosch process, also known as pulsed or time-multiplexed etching alternates repeatedly between two modes to achieve nearly vertical structures. First a standard, nearly isotropic plasma etch is used. The plasma contains some ions, which attack the wafer from a nearly vertical direction. Sulfur hexafluoride SF_6 is often used for silicon. Second is the deposition of a chemically inert passivation layer.

Each phase lasts for several seconds. The passivation layer protects the entire substrate from further chemical attack and prevents further etching. However, dur-

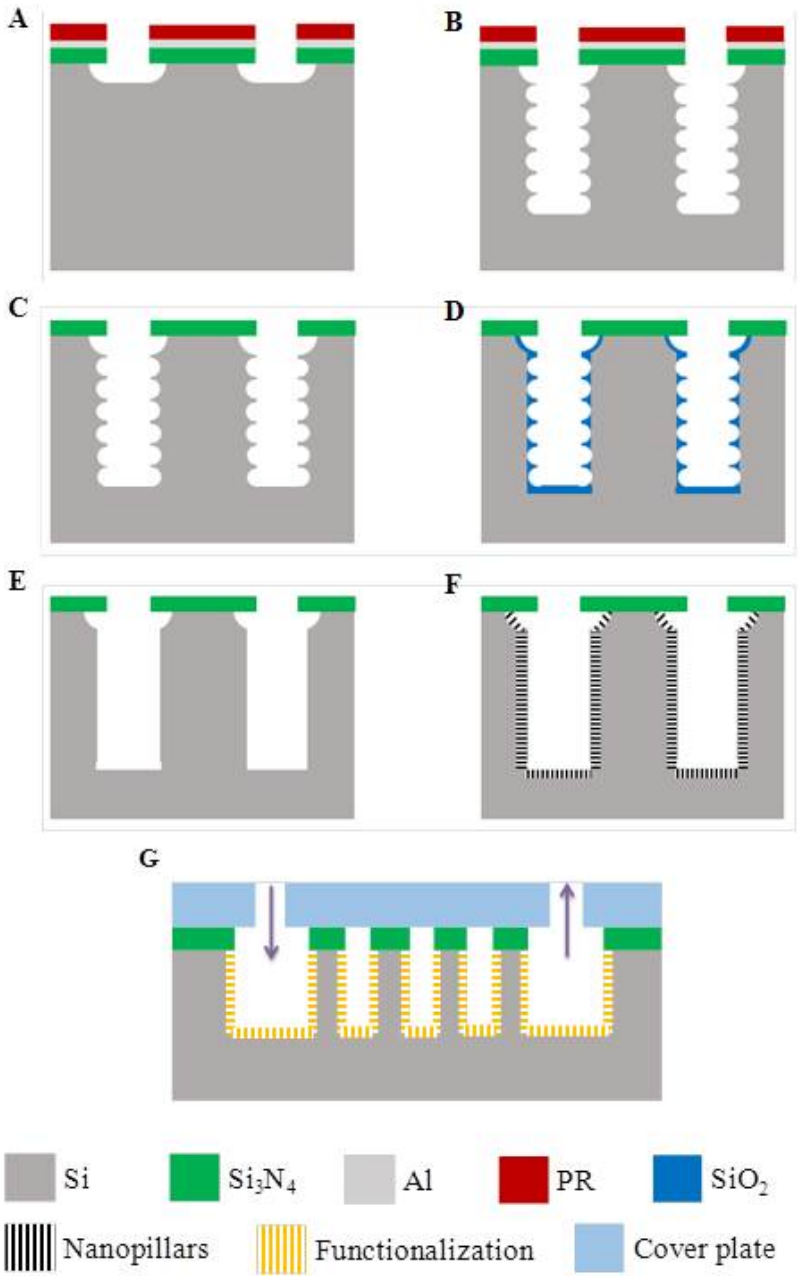

Figure 4.2. Schematic of steps involved in the fabrication process [15].

ing the etching phase, the directional ions that bombard the substrate attack the passivation layer at the bottom of the trench (but not along the sides). They collide with it and sputter it off, exposing the substrate to the chemical etchant.

These etch/deposit steps are repeated many times over resulting in a large number of very small isotropic etch steps taking place only at the bottom of the etched pits. To etch through a 0.5 mm silicon wafer, for example, 1001000 etch/deposit steps are needed. The two-phase process causes the sidewalls to undulate with an amplitude of about 100500 nm. The cycle time can be adjusted: short cycles yield smoother walls, and long cycles yield a higher etch rate. This step is depicted in Fig. 4.2(B).

Step 3: This is shown in Fig. 4.2(C). Prior to growing nanostructures on the surface of micro posts, the photoresist and aluminum were removed, and polymer residues from the DRIE process were subjected to Piranha cleaning and ashing in oxygen plasma.

Piranha solution, also known as piranha etch, is a mixture of sulfuric acid (H_2SO_4) and hydrogen peroxide (H_2O_2), used to clean organic residues off substrates. Because the mixture is a strong oxidizing agent, it will remove most organic matter, and it will also hydroxylate most surfaces, making them highly hydrophilic.

Many different mixture ratios are commonly used, and all are called piranha. A typical mixture is 3:1 concentrated sulfuric acid to 30% hydrogen peroxide solution; other protocols may use a 4:1 or even 7:1 mixture. A closely related mixture, sometimes called "base piranha", is a 3:1 mixture of ammonium hydroxide (NH_4OH) with hydrogen peroxide.

Piranha solution must be prepared with great care. It is highly corrosive and an extremely powerful oxidizer. Surfaces must be reasonably clean, and completely free of organic solvents from previous wash steps, before coming into contact with piranha solution. Piranha solution cleans by dissolving organic contaminants, and a large amount of contaminant will cause violent bubbling and a release of gas that can cause an explosion. Piranha solution may be prepared by adding the peroxide to the acid. Mixing the solution is exothermic. The resultant heat can bring solution temperatures up to 120°C. It must be allowed to cool reasonably before applying any heat. The sudden increase in temperature can also lead to violent boiling, or even splashing of the extremely acidic solution. Also, explosions may occur if the peroxide

solution concentration is more than 50%. Once the mixture has stabilized, it can be further heated to sustain its reactivity. The hot (often bubbling) solution will clean organic compounds off substrates, and oxidize or hydroxylate most metal surfaces. Cleaning usually requires about 10 to 40 minutes, after which time the substrates can be removed from the solution.

The solution may be mixed before application or directly applied to the material, applying the sulfuric acid first, followed by the peroxide. Due to the self-decomposition of hydrogen peroxide, piranha solution should be used freshly prepared.

Step 4: Surface quality being critical for nanopillar synthesis, a short oxidation step in a tube furnace at 1100°C was employed in order to treat the scallop sidewall roughness on micro posts. This is shown in Fig. 4.2(D).

Step 5: Subsequently, the oxide was etched, and the silicon nitride was to serve as a protective mask for the top surfaces during nanopillar fabrication as shown in Fig. 4.2(E)

Step 6: Silicon Nanopillars were synthesized on the surface of the micro posts and microchannel walls by an aqueous electroless metal assisted chemical etching (MACEtch) method using Ag+/HF solutions as depicted in Fig. 4.2(F).

Step 7: The surface of the micro posts in the microchannel was functionalized with aptamers and capped for experiments as shown in Fig. 4.2(G).

Step 8: Aptamer binding on silicon dioxide surface was carried out by a well-known click chemistry, as shown in the schematic in Fig. 4.3.

The traditional process of drug discovery based on natural secondary metabolites has often been slow, costly, and labor-intensive. Even with the advent of combinatorial chemistry and high-throughput screening in the past two decades, the generation of leads is dependent on the reliability of the individual reactions to construct the new molecular framework.

Click chemistry is a newer approach to the synthesis of drug-like molecules that can accelerate the drug discovery process by utilizing a few practical and reliable reactions.

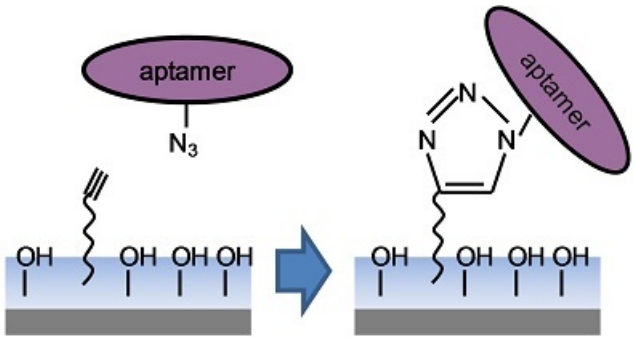

Figure 4.3. Schematic of the click chemistry process for functionalizing surfaces with aptamers [15].

Sharpless and coworkers defined what makes a click reaction as one that is wide in scope and easy to perform, uses only readily available reagents, and is insensitive to oxygen and water. In fact, in several instances water is the ideal reaction solvent, providing the best yields and highest rates. Reaction work-up and purification uses benign solvents and avoids chromatography.

Previously, MACEtching has been demonstrated using a variety of oxidizers and etchants for flat substrates. In this work, a new development is the technique of etching Silicon Nanopillars into the sidewalls of DRIE patterned surfaces, which facilitates the development of truly hierarchical micro/nanostructures and nanoscale patterning along preferred crystal directions. Fig. shows Silicon Nanopillars that have been etched into the sidewalls of test structures comprised of circular micro posts that are 50 m deep. In both cases, the micro posts demonstrate complete Silicon Nanopillars coverage and the evolution of the nanopillars is along the <100> crystal direction as seen by the tangential planes to the circular post.

Advantage of Silicon Nanopillars: The present work incorporates the use of a Silicon Nanopillar forest that is grown on the solid micropost giving rise to a structure that contains a solid core with a kind of porous sheath covering. As we have seen in the literature of this field, one particular design used vertically aligned carbon nanotubes (VACNT). Though this device did tend to give high capture efficiency, the device reusability was questionable. This is because, when compared to Silicon Nanopillars,

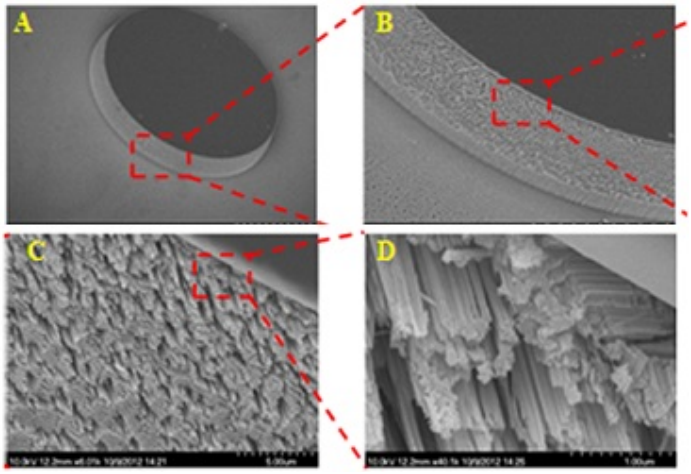

Figure 4.4. SEM images of MAC Etched Silicon Nano Pillars fabricated on sidewall surfaces of (A–*D*) circular micro posts along <100> planes [15].

VACNT are relatively longer and therefore provide a high susceptibility of being sheared or broken off when the sample flows through it at high velocity (microscale based). This particular setback results in low throughput and limited reusability of the device. Silicon Nanopillars accounts for this draw back and therefore increases the yield of the device.

5. CONCLUSIONS

5.1 Design Optimization

The microfluidic device has been studied and optimized to produce higher capture efficiency of the rare cells. The performance of rare cell-capture devices, as measured by capture efficiency and sample purity, is primarily affected by two phenomena: the chemical interaction between the cell and the capture surface and the transport of cells to (and their collision dynamics with) the capture surface. Modern rare cell immunocapture devices use both chemical and fluid-dynamic optimization to maximize the efficiency and purity of capture.

As noted from previous studies, the use of solid cylinders as microposts not only increased the hydrodynamic resistance between the cell and the post wall but also led to lower capture efficiency. To overcome this limitation we incorporated a porous shell around the solid cylinder. The porous shell has contributed to a lot of factors in optimizing the design of the microfluidic chip. Due to the porous shell, the hydrodynamic resistance between the cell and post wall has reduced significantly. The shear stress in flow field has reduced and there is a much noticeable drop in the drag coefficient when compared to the design that uses only solid cylinders.

The permeability of the shell plays an important role in affecting the above mentioned parameters. High permeability leads to more allowance of fluid through the porous shell and thereby increasing the contact efficiency between the cell and wall. The shear stress around the post is also greatly reduced.

The posts arrangement is one of the most important aspects and contributions to the increase in capture efficiency. We started off with an initial equilateral triangle arrangement and then later made modifications to it by shifting some columns of microposts. Obstacle arrays have several properties that lend themselves to microfluidic

cell transport applications. The rational array geometry, lends itself to parametric engineering design studies, and can be optimized to control particle motion and particle–obstacle collision dynamics. The large number of posts in the array results in a system that is robust to local flow disruptions caused by fabrication errors and inlet and outlet conditions.

Flow near surfaces induces few cell-wall collisions when the no-penetration condition is satisfied; this boundary condition limits collision frequency but provides opportunities to optimize performance by using the fluid mechanics to enhance purity based on mechanical properties of the cells. Porous surfaces with finite penetration tend to maximize capture efficiency but do not add a fluid-specific purification.

Mechanical property variation, most importantly size differences between target and nontarget cells, can be leveraged to create size-dependent transport and collision dynamics. Because steric interactions with surfaces are often the dominant source of cell motion across streamlines, bluff-body obstacles are simultaneously the simplest way to induce collision and generate size-dependent transport across streamlines. In some systems, size-dependent transport can be used to increase purity and therefore enhance overall device capture efficiency.

It is desirable to have a higher yield for such devices. After optimizing the microfluidic chip, we have obtained a design that tends to three main requirements viz. higher capture efficiency, higher yield and lower shear stress in the flow as compared to devices using only solid cylinders as microposts. The optimized design allowed for retaining high capture efficiencies even with an increase in inlet velocity. This particular aspect of the chip will help reduce the functioning time when applied for practical purposes.

5.2 Future Work

The field of microfluidic has a promising future and finds tremendous potential in many applications. One such field is the study that has been presented in this

research work. A device used for rare cell separation and its study is a topic of immense interest and is attracting more researchers and users alike.

The future work of this study would be the inclusion of some parameters that have been kept aside for a more simplistic approach of the work. We have assumed throughout the study that the working fluid, blood, is a Newtonian fluid and takes on the properties of water. We have done so to ignore the complexities that may arise due to the nonlinear relationship between the shear stress and strain rates. During the later works of this study, the Non Newtonian behavior of blood can be taken into consideration.

The molecular interaction between the cell surface and the post wall can be studied more extensively. The cancer cell surface consists of Microvilli and Filopodia and the post wall has nanowires grown on them. The interaction between the cell surface and post surface and the molecular dynamics involved can be more extensively studied.

Also, the fluid is assumed as a continuum. The interaction between the particles of the fluid is left for more complex studies as it would involve inter particle collision dynamics and an entire new study can be designed only to observe these effects. In the study presented in this work the particle velocity is the same as the fluid velocity and therefore avoiding the expense of accounting for different particle velocities.

This work consists of a theoretical approach and is supported by CFD simulations. A commendable continuation to this present study would be to have experimental validation and compare the results obtained from them with the results achieved by the simulations.

LIST OF REFERENCES

LIST OF REFERENCES

[1] S. Wang and K. Liu, "Highly Efficient Capture of Circulating Tumor Cells by Using Nanostructured Silicon Substrates with Integrated Chaotic Micromixers," in *Angewandte Chemie International Edition.*, vol. 50(13), 2011, pp. 3084-3088.

[2] Y. Taamneh and K. M. Bataineh, "Drag and Separation Flow Past Solid Sphere with Porous Shell at Moderate Reynolds Number," in *Transport in Porous Media.*, vol. 90(3), 2011, pp. 869-881.

[3] A. C. Srivastava and N. Srivastava, "Flow of a viscous fluid at small Reynolds number past a porous sphere with a solid core," in *Acta Mechanica.*, vol. 186(1-4), 2006, pp. 161-172.

[4] S. Nagrath et al., "Isolation of rare circulating tumour cells in cancer patients by microchip technology," in *Nature.*, vol. 450(7173), 2007, pp. 1235-1239.

[5] A. D. Hughes and M. R. King, "Nanobiotechnology for the capture and manipulation of circulating tumor cells," *Wiley Interdisciplinary Reviews: Nanomedicine and Nanobiotechnology.*, vol. 4(3), pp. 291-309, 2012.

[6] L. R. Huang "Continuous Particle Separation Through Deterministic Lateral Displacement," *Science.*, vol. 304(5673), pp. 987-990, 2004.

[7] T. Grosan et al., "Brinkman Flow of a Viscous Fluid Through a Spherical Porous Medium Embedded in Another Porous Medium," *Transport in Porous Media.*, vol. 81(1), pp. 89-103, 2009.

[8] J. P. Gleghorn et al., "Capture of circulating tumor cells from whole blood of prostate cancer patients using geometrically enhanced differential immunocapture (GEDI) and a prostate-specific antibody," *Lab on a Chip.*, vol. 10(1), pp. 27-29, 2010.

[9] S.Deo and P. K. Yadav, "Stokes Flow past a Swarm of Porous Nanocylindrical Particles Enclosing a Solid Core," *International Journal of Mathematics and Mathematical Sciences.*, pp. 1-8, 2008.

[10] G. D. Chen et al., "Nanoporous micro-element arrays for particle interception in microfluidic cell separation," *Lab on a Chip.*, vol. 12(17), pp 31-59, 2012.

[11] A. Bhattacharya and G. P. Raja Sekhar, "Potential Flow Past a Slightly Deformed Porous Circular Cylinder," *Transport in Porous Media.*, vol. 81, pp. 367-389, 2009.

[12] A. Thomas et al., "Micro-patterned surface for efficient capturing of circulating tumor cells," in *Bioengineering Conference (NEBEC) 38th Annual Northeast.*, 2012.

[13] Y. Taamneh and K. M. Bataineh, "Drag and Separation Flow Past Solid Sphere with Porous Shell at Moderate Reynolds Number," in *Transport in Porous Media.*, vol. 90(3), 2011, pp. 869-881.

[14] A. C. Srivastava and N. Srivastava, "Flow of a viscous fluid at small Reynolds number past a porous sphere with a solid core," in *Acta Mechanica.*, vol. 186(1-4), 2006, pp. 161-172.

[15] Vikhram V. Swaminathan, Spandana Gannavaram, Shihui Li, Huan Hu, Junghoon Yeom, Yong Wang, and Likun Zhu, "Microfluidic Platform with Hierarchical Micro/Nanostructures and SELEX Nucleic Acid Aptamer Coating for Isolation of Circulating Tumor Cells", presented at IEEE nanotechnology, Beijing, China, 2013.

[16] J. Prakash and G. P. Raja Sekhar, "Estimation of the dynamic permeability of an assembly of permeable spherical porous particles using the cell model," *Journal of Engineering Mathematics.*, vol. 80(1), pp. 63-73, 2013.

[17] H. Power and P. Tyvand, "Drag force and virtual mass of a cylindrical porous shell in potential flow," in *Zeitschrift fr angewandte Mathematik und Physik ZAMP*, Vol. 43(6), 1992, pp. 1055-1071.

[18] I. Pop and P. Cheng, "Flow past a circular cylinder embedded in a porous medium based on the brinkman model," *International Journal of Engineering Science.*, vol. 30(2), pp. 257-262, 1992.

[19] J. A. Phillips et al., "Enrichment of Cancer Cells Using Aptamers Immobilized on a Microfluidic Channel," *Analytical Chemistry.*, vol. 81(3), pp. 1033-1039, 2008.

[20] P. D. Noymer et al., "Drag on a permeable cylinder in steady flow at moderate Reynolds numbers." *Chemical Engineering Science.*, vol. 53(16), pp. 2859-2869, 1998.

[21] H. Lu et al., "Microfluidic Shear Devices for Quantitative Analysis of Cell Adhesion." *Analytical Chemistry.*, vol. 76(18), pp. 5257-5264, 2004.

[22] S. Kuwabara, "The Forces experienced by Randomly Distributed Parallel Circular Cylinders or Spheres in a Viscous Flow at Small Reynolds Numbers," *Journal of The Physical Society of Japan.*, vol. 14(4), pp. 527-532, 1959.

[23] A. D. Hughes and M. R. King, "Nanobiotechnology for the capture and manipulation of circulating tumor cells," *Wiley Interdisciplinary Reviews: Nanomedicine and Nanobiotechnology.*, vol. 4(3), pp. 291-309, 2012.

[24] L. R. Huang "Continuous Particle Separation Through Deterministic Lateral Displacement," *Science.*, vol. 304(5673), pp. 987-990, 2004.

[25] H. W. Hou et al., "Isolation and retrieval of circulating tumor cells using centrifugal forces," *Scientific Reports.*, 2013.

[26] J. Happel, "Viscous flow relative to arrays of cylinders," *AIChE Journal.*, vol. 5(2), pp. 174-177, 1959.

[27] T. Grosan et al., "Brinkman Flow of a Viscous Fluid Through a Spherical Porous Medium Embedded in Another Porous Medium," *Transport in Porous Media.*, vol. 81(1), pp. 89-103, 2009.

[28] J. P. Gleghorn et al., "Capture of circulating tumor cells from whole blood of prostate cancer patients using geometrically enhanced differential immunocapture (GEDI) and a prostate-specific antibody," *Lab on a Chip.*, vol. 10(1), pp. 27-29, 2010.

[29] F. Fachin et al., "Integration of Bulk Nanoporous Elements in Microfluidic Devices With Application to Biomedical Diagnostics," *Microelectromechanical Systems, Journal of.*, vol. 20(6), pp. 1428-1438, 2011.

[30] S.Deo and P. K. Yadav, "Stokes Flow past a Swarm of Porous Nanocylindrical Particles Enclosing a Solid Core," *International Journal of Mathematics and Mathematical Sciences.*, pp. 1-8, 2008.

[31] N. S. Cheng, "Calculation of Drag Coefficient for Arrays of Emergent Circular Cylinders with Pseudofluid Model," *Journal of Hydraulic Engineering.*, vol. 139(6), pp. 602-611, 2013.

[32] G. D. Chen et al., "Nanoporous micro-element arrays for particle interception in microfluidic cell separation," *Lab on a Chip.*, vol. 12(17), pp 31-59, 2012.

[33] S. Bhattacharyya et al., "Fluid motion around and through a porous cylinder," *Chemical Engineering Science.*, vol. 61(13), pp. 4451-4461, 2006.

[34] A. Bhattacharya and G. P. Raja Sekhar, "Potential Flow Past a Slightly Deformed Porous Circular Cylinder," *Transport in Porous Media.*, vol. 81, pp. 367-389, 2009.

[35] L. A.Spielman, "Particle Capture from Low-Speed Laminar Flows," *Annual Review of Fluid Mechanics.*, vol. 9(1), pp. 297-319, 1977.

[36] G. Yao and W. Tan, "Molecular-beacon-based array for sensitive DNA analysis," *Anal Biochem.*, vol. 331(2), pp. 216-223, 2004.

[37] H. Xie et al., "EGF receptor regulation of cell motility: EGF induces disassembly of focal adhesions independently of the motility-associated PLCgamma signaling pathway," *J Cell Sci.*, pp. 615-624, 1998.

[38] M. Wolf et al., "Screening cell surface receptors using micromosaic immunoassays," *Biomed Microdevices.*, vol. 9(2), pp. 135-141, 2007.

[39] C. Yi et al., "Microfluidics technology for manipulation and analysis of biological cells," *Analytica Chimica Acta.*, vol 560(12), pp. 1-23, 2006.

[40] C. Y. Wang, "Stokes slip flow through square and triangular arrays of circular cylinders," *Fluid Dynamics Research.*, vol. 32(5), pp. 233, 2003.

[41] A. D. Hughes and M. R. King, "Nanobiotechnology for the capture and manipulation of circulating tumor cells," *Wiley Interdisciplinary Reviews: Nanomedicine and Nanobiotechnology.*, vol. 4(3), pp. 291-309, 2012.

[42] J. A. Phillips et al., "Enrichment of Cancer Cells Using Aptamers Immobilized on a Microfluidic Channel," *Analytical Chemistry.*, vol. 81(3), pp. 1033-1039, 2008.

[43] L. R. Huang "Continuous Particle Separation Through Deterministic Lateral Displacement," *Science.*, vol. 304(5673), pp. 987-990, 2004.

[44] D. L. Vickers et al., "Lectin-mediated microfluidic capture and release of leukemic lymphocytes from whole blood," *Biomedical Microdevices.*, vol. 13(3), pp. 565-571, 2011.

[45] A. Thomas et al., "Micro-patterned surface for efficient capturing of circulating tumor cells," in *Bioengineering Conference (NEBEC) 38th Annual Northeast.*, 2012.

[46] C. Yi et al., "Microfluidics technology for manipulation and analysis of biological cells," *Analytica Chimica Acta.*, vol 560(12), pp. 1-23, 2006.